Mon. Not. R. Astron. Soc. **263**, 1023–1048 (1993)

The radio structures of southern 2-Jy radio sources

R. Morganti,[1] N. E. B. Killeen[2] and C. N. Tadhunter[3]
[1] *Istituto di Radioastronomia, via Irnerio 46, I-40126 Bologna, Italy*
[2] *Australia Telescope National Facility, CSIRO, PO Box 76, Epping, NSW 2121, Australia*
[3] *Department of Physics, University of Sheffield, Sheffield S3 7RH*

Accepted 1993 February 12. Received 1993 February 8; in original form 1992 October 5

ABSTRACT

A subsample of the Wall & Peacock 2-Jy sample of radio sources, with redshift $z < 0.7$ or unknown and declination $\delta < +10°$, has been selected and observed in the radio at 6 cm (or information was obtained from the literature where appropriate) and in the optical with low-dispersion spectroscopy. Here we present the new radio data. We observed 66 sources with the Very Large Array and seven southern sources with the Australia Telescope Compact Array. Together with the data collected from the literature, we now have information about the radio structure of 107 sources. These data will be discussed along with optical spectra for the sample in a future paper.

Key words: galaxies: active – radio continuum: galaxies.

1 INTRODUCTION

Many recent studies have revealed relationships between the optical and radio properties in both high- and low-luminosity radio sources (e.g. Baum & Heckman 1989; Rawlings et al. 1989; Morganti, Ulrich & Tadhunter 1992), but the true nature of these relationships remains controversial. For example, do the radio plasma and the UV ionizing continuum have a common origin, and what are the effects of interactions between the radio plasma and the interstellar medium? In addition to this, in the framework of 'unified schemes', both radio and spectroscopic data have been used as possible indicators of the orientation of the beamed radiation with respect to the line of sight [i.e. the parameter $R = S_{\rm core}/(S_{\rm tot} - S_{\rm core})$, obtained from the radio data, the presence of broad and narrow lines from the optical data]. Up to now, these two 'orientation'-dependent indicators as a test for the 'unified schemes' have been compared mainly using samples of quasars (see Jackson & Browne 1991 and references therein); it would be useful to have a similar study for a sample formed from both radio galaxies and quasars.

Since these two topics are worthy of further investigation, we have started a major survey of optical and radio observations of southern radio sources. In this, the second of a series of papers concerned with our survey, we present the radio data. The optical spectroscopic data are in Paper I (Tadhunter et al. 1993), while the new redshifts and optical identifications made in the course of our survey will be presented in Paper III (de Serego Alighieri et al., in preparation).

The overall aims of our survey can be summarized as follows (see also Paper I):

(i) to attempt to understand the underlying physical cause(s) of the optical/radio correlations, and to investigate the dependence of the correlation on the detailed optical and radio properties and the way the samples have been selected;
(ii) to investigate the reliability of the orientation parameters (like R) used in 'unified schemes';
(iii) to investigate the nature of compact steep-spectrum radio sources and their relationship to other types of radio source;
(iv) to improve the status of the optical identifications of southern radio sources. A large fraction of the sources from the Wall & Peacock (1985) 2-Jy sample lacked spectroscopic identification prior to our survey.

The optical and radio data, for the complete sample described in Paper I, will be discussed together in Paper IV (Tadhunter et al., in preparation). Here we present the results of our 6-cm Very Large Array (VLA) observations for 66 sources with $-35° \leq \delta < +10°$, our 6-cm Australia Telescope Compact Array (ATCA) observations for seven sources with $\delta < -35°$, and information from the literature on the remaining sources. The main quantities derived from these data are the radio core flux density and the morphological description [i.e. Fanaroff & Riley-type (Fanaroff & Riley 1974), core-dominated, compact steep-spectrum (CSS), etc.].

2 THE SAMPLE

The main goal of these new observations is to collect radio and spectroscopic data for a *complete sample* of radio sources selected from the Wall & Peacock (1985, hereafter

WP85) 2.7-GHz sample with the following criteria: declination $\delta \leq +10°$ and redshift $z < 0.7$. This sample is complete down to a flux density of 2 Jy. Its main advantage (as discussed by Peacock & Wall 1982 for a similarly selected northern sample) is that, being a relatively high-frequency sample, it contains a good mixture of flat-spectrum and steep-spectrum sources, extended and CSS radio galaxies, and quasars. In order to obtain this complete sample we have selected for observations all the 67 objects in the WP85 sample with known redshift that fulfil the above criteria *and* the objects with $\delta \leq +10°$ for which no spectroscopic redshifts and no optical identifications are given in WP85. We include these objects to ensure that the final sample is complete.

According to the classification given by WP85 (and new information collected from our optical data), the sample contains 83 galaxies (including 10 uncertain cases), 25 quasars (including five uncertain cases) and two empty fields. The data presented here (either new observations or data collected from literature) concern 107 objects of the initial sample. As discussed in Paper I, not all these sources belong to the final 'complete sample' (i.e. objects with $z < 0.7$). In fact, using the new measured redshifts, the sample that is considered largely 'complete' (see the discussion in Paper I about completeness) is formed by 87 objects listed in table 2 of Paper I.

In this paper we have assumed $H_0 = 50$ km s^{-1} Mpc^{-1} and $q_0 = 0$. All positions are for epoch 1950.0.

3 THE RADIO DATA

3.1 The VLA observations

Table 1 lists the observed objects. 65 objects of the sample were observed with the VLA in 1989 May and September at 4.885 GHz with a bandwidth of 50 MHz, using either the C or the C+B_N hybrid configuration. This subsample consists of all the objects with declinations in the range $-35° < \delta < 10°$. For six objects in the sample (3C 75, 3C 105, 3C 273, Her A, 3C 403 and 3C 445), observations with the same resolution were already available in literature (see Section 3.4). The C configuration was used for the objects with $-20° < \delta < +10°$, and the hybrid C+B_N configuration (which partly compensates for the beam elongation at southern declinations) was used for the remaining objects. For one object (NGC 612 = 0131 − 36), data taken by one of the authors (N. Killeen) with the D+C_N configuration in 1985 are presented.

We used 3C 48 and 286 as primary flux density calibrators and adopted the flux density scale of Baars et al. (1977). Each object was observed for about 10–15 min, and an observation of a secondary flux calibrator followed that of each source. After calibration, the sources were imaged using NRAO's Astronomical Image Processing System (AIPS). We used the Clark (1980) CLEAN algorithm (as implemented in the Cotton-Schwab 'MX' algorithm). For all the sources, self-calibration (Schwab 1980) was also used to remove residual antenna-based complex gain errors. In Table 1 we also list the configuration used for each object, the synthesized beam obtained (typically a FWHM of between 3 and 6 arcsec), the noise of the final image, the total flux density measured, and the percentage of the 'total power flux density' (from WP85) that this represents. The latter quantity gives an idea of how much flux density is lost because of the relatively high resolution of the observations compared with the dimensions of some of the sources. In a few objects, the measured flux density is higher than the 'total power flux'; these cases (indicated by >) are probably variable (see also Section 3.4).

After self-calibration, the dynamic range (ratio of peak to rms noise) of the image is, in many cases, better than 1000 to 1. Since the sample is dominated by strong sources which often contain compact components, the observations were dynamic-range-limited. However, for the large sources in our sample, especially those with diffuse structures, the inadequate sampling is a more serious problem. In such cases the dynamic range is no better than 100 to 1.

3.2 The ATCA observations

For most of the sources with $\delta < -35°$, information could be collected from the literature (see Section 3.3), but there were seven sources without high-resolution images which we observed with the ATCA (see Table 2): 0427 − 53, 0629 − 52, 1318 − 43, 1637 − 77, 1733 − 56, 1839 − 48 and 2250 − 41.

The observations were made on 1991 December 12 with a 1.5-km configuration, and on 1992 April 2 with a 3-km configuration. We took data simultaneously at 4.74 and 5.70 GHz, each with a bandwidth of 128 MHz. These separated frequencies enabled us to enhance (radially) the instantaneous *uv* coverage which is limited by the six-telescope east–west Compact Array.

The flux-density scale was set by observations of 1934 − 638 (which we assumed to be 6.44 and 4.99 Jy at 4.74 and 5.70 GHz, respectively). Each source was observed about 8 to 10 times (for about 15 min) throughout each 24-h observing period to ensure good hour-angle coverage. These observations were interspersed with secondary calibrators for basic complex gain calibration. Finally, 10 min of data on the linear polarization position calibrator 3C138 were also obtained.

The ATCA correlator produces 32 channels across the 128-MHz band, but in the analysis we chose to average together the central 20 channels at each of the two frequencies because the benefit of gridding all the channels in the *uv* plane is modest at this frequency and bandwidth ($\delta\nu/\nu < 2$ per cent).

The data were edited in the AIPS package, following which they were removed to the MIRIAD package (developed by the Berkeley-Illinois-Maryland software consortium) for calibration and imaging. We used MIRIAD because this is where the ATCA gain and polarimetric calibration code has been developed (Sault, Killeen & Kesteven 1991). Note that, although we do not present polarized intensity images, it is still necessary to make a polarization calibration for linear feeds to get the total intensity correct.

Following basic gain and polarization calibration, the 4.74- and 5.70-GHz data from both configurations were concatenated and imaged in MIRIAD. Here we took advantage of the multi-frequency synthesis alogrithms recently developed at the Australia Telescope National Facility (Sault 1992; see also Conway, Cornwell & Wilkinson 1990). These extend from the Fourier inversion of the visibilities to the

Table 1. 2-Jy sample – VLA observations.

Object	Other Name	Array	Resolution (P.A.) arcsec (degrees)	rms mJy	S_{tot} Jy	%	Object	Other Name	Array	Resolution (P.A.) arcsec (degrees)	rms mJy	S_{tot} Jy	%
0023 − 26	OB-238	B/C	5.3x3.0(−57°)	0.2	3.410	1.00	0915 − 11	HydA	C	5.1x3.8(+1°)	2.4	11.505	0.84
0034 − 01	3C15	C	4.1x3.7(−28°)	0.3	1.583	0.95	0945 + 07	3C227	C	3.9x3.9(−33°)	0.8	2.072	0.79
0035 − 02	3C17	C	4.0x3.6(−31°)	0.2	2.416	0.92	1015 − 31	OL-327	B/C	2.3x2.3(+45°)	0.6	1.370	1.00
0038 + 09	3C18	C	3.5x3.2(−36°)	0.1	1.729	1.00	1136 − 13	OM-161	C	5.1x3.3(−13°)	1.1	1.373	0.72
0045 − 25	NGC253	B/C	5.3x3.0(−57°)	0.5	1.085	0.45	1151 − 34	OM-386	B/C	3.3x3.0(+35°)	1.9	2.620	0.94
0055 − 01	3C29	C	3.8x3.5(−34°)	0.5	1.332	0.61	1216 + 06	3C270	C	4.1x3.5(−12°)	0.6	1.390	0.07
0105 − 16	3C32	C	4.7x2.0(−70°)	0.1	1.024	0.88	1245 − 19	ON-176.2	C	3.6x2.1(+88°)	0.7	2.360	0.94
0114 − 21	OC-224	B/C	4.5x2.3(−69°)	0.5	1.178	0.93	1251 − 12	3C278	C	5.0x3.2(−17°)	0.3	1.622	0.65
0117 − 15	3C38	C	4.3x1.9(−79°)	0.4	1.328	0.83	1253 − 05	3C279	C	4.6x3.4(−15°)	3.0	11.580	0.73
0123 − 01	3C40	C	3.9x3.5(−31°)	0.1	0.156	0.08	1306 − 09	OP-10	C	4.8x3.3(−16°)	0.5	1.913	1.00
0131 − 36	NGC612	C/D	10.1x8.0(+15°)	0.1	1.180	0.29	1308 − 22	3C283	B/C	3.5x2.2(+87°)	0.5	1.160	1.00
0157 − 31	OC-397	B/C	4.8x3.6(−54°)	0.6	1.110	0.76	1333 − 33	IC4296	B/C	3.4x3.3(−34°)	0.3	0.838	0.08
0159 − 11	3C57	C	4.5x3.3(−22°)	0.4	1.208	0.88	1510 − 08	OR-107	C	4.7x3.3(−14°)	0.5	1.613	0.50
0213 − 13	3C62	C	4.5x3.2(−22°)	0.2	1.720	0.96	1514 + 07	3C317	C	3.5x3.2(−33°)	0.2	0.864	0.90
0235 − 19	OD-159	C	4.5x2.2(−70°)	0.2	1.180	0.82	1514 − 24	ApLib	B/C	4.8x4.4(+40°)	0.2	1.530	0.79
0240 − 00	NGC1068	C	3.9x3.7(−34°)	0.2	1.620	0.82	1518 + 04	4C04.51	C	3.6x3.3(−34°)	0.4	1.045	1.00
0305 + 03	3C78	C	3.9x3.5(−31°)	0.8	2.356	0.65	1559 + 02	3C327	C	3.6x3.3(−34°)	0.4	1.911	0.67
0325 + 02	3C88	C	3.9x3.5(−31°)	0.3	1.118	0.56	1602 + 01	3C327.1	C	3.7x3.3(−33°)	0.6	1.071	0.95
0347 + 05	4C05.16	C	3.8x3.4(−30°)	0.5	1.091	0.87	1622 − 25	OS-237.8	B/C	5.4x3.9(+29°)	0.2	3.077	>
0349 − 27	OE-283	B/C	6.8x3.8(−52°)	0.3	0.743	0.36	1717 − 00	3C353	C	3.7x3.5(−36°)	2.6	10.530	0.52
0403 − 13	OF-105	C	4.5x3.2(−23°)	1.0	2.805	0.86	1938 − 15	OV-164	C	6.1x3.0(−11°)	0.6	2.450	1.00
0405 − 12	OF-109	C	4.5x3.3(−22°)	0.8	1.280	0.70	2008 − 06	OW-15	C	4.3x3.6(−28°)	0.6	1.306	0.97
0430 + 05	3C120	C	3.6x3.4(−36°)	1.4	3.930	0.46	2058 − 28	OW-297.8	B/C	7.4x2.8(−11°)	0.4	0.467	0.23
0442 − 28	OF-271	B/C	8.7x4.3(−50°)	1.1	1.673	0.76	2104 − 25	OX-208	B/C	7.4x2.9(−10°)	0.3	0.634	0.15
0453 − 20	OF-289	B/C	6.2x2.5(+44°)	0.5	1.424	0.79	2128 + 04	OX46	C	3.3x3.2(−42°)	0.5	1.981	0.96
0500 + 01	OG3	C	4.3x4.2(+44°)	0.2	1.997	1.00	2128 − 12	OX-148	C	4.5x3.3(−21°)	1.0	2.821	>
0605 − 08	OH-10	C	5.1x4.1(+23°)	0.6	2.540	0.76	2135 − 14	OX-158	C	5.0x3.4(−14°)	0.3	1.306	0.95
0736 + 01	OI61	C	4.1x3.9(−33°)	0.2	1.905	0.95	2135 − 20	OX-20	B/C	6.3x3.0(−12°)	0.2	1.379	0.90
0806 − 10	3C195	C	5.2x3.8(+5°)	0.2	1.358	0.83	2203 − 18	OY-106	C	6.1x3.0(−13°)	0.8	3.970	0.93
0825 − 20	OJ-242	B/C	4.9x2.7(+56°)	0.8	1.191	0.99	2211 − 17	3C444	C	6.0x3.0(−22°)	0.4	1.430	0.67
0834 − 19	OJ-158.1	C	5.1x2.8(+56°)	1.1	1.488	0.97	2243 − 12	OY-172.6	C	4.5x3.3(−22°)	0.6	2.297	0.97
0858 − 27	OJ-297	B/C	6.0x4.3(+49°)	2.0	2.210	>	2314 + 03	3C459	C	3.5x3.3(−40°)	0.4	1.255	0.94
0859 − 25	OJ-299	B/C	6.5x3.8(+50°)	0.8	1.360	0.78	2345 − 16		C	5.7x2.9(−16°)	0.2	1.925	0.55

deconvolution via a Clark CLEAN and self-calibration. These algorithms deal with the fact that the spectral index of the source may not be zero, so that the images are not compromised by the widely separated frequencies. In addition, the frequency-dependent primary beam differential between 4.74 and 5.7 GHz masquerades as a spectral index effect, so that it too is dealt with. This may be important for large sources such as those we are imaging. Finally, a spectral index image is a standard result of the procedure. The only drawback to using the multi-frequency algorithms is that they add the extra unknown of the spectral index to the deconvolution process. Our tests indicated that we could make better images with the multi-frequency algorithms than with the standard procedure where one assumes that the spectral index is zero.

Self-calibration (both in amplitude and in phase) was applied to the data. One must be careful when self-calibrating ATCA data, because the instantaneous *uv* coverage is only one-dimensional and because the problem of solving for the antenna gains is only slightly over-determined (4.5 complex gains from 10 baselines). It is crucial that the initial model be as good as possible so that the procedure converges reasonably quickly (see Sault 1991). This is why we start by combining all data from all configurations and frequencies so as to make the best possible initial model with which to proceed in the self-calibration process.

3.3 Additional data from the literature

In addition to the 66 objects observed with the VLA and the seven observed with the ATCA, we have collected information from the literature or from unpublished data for the majority of the remaining objects. Although low-resolution data may exist for many of these objects [see, for example, Jones & McAdam (1992) for data obtained with the Molonglo Synthesis Telescope (MOST)], we have tried to select the data which have similar resolution and sensitivity to our VLA and ATCA observations. In some uncertain cases we have used the low-resolution map only for the morphological classification of the objects.

The references relevant for the single objects are given in the notes on the sources (see 'Notes on individual sources' in

Table 2. 2-Jy sample – ATCA observations.

Object	Other Name	Resolution (P.A.) arcsec (degrees)	rms mJy	S_{tot} Jy	%
0427 – 53		2.7x1.4(+16°)	0.52	0.94	0.28
0620 – 52		4.7x2.7(+2°)	0.50	1.31	1.00
1318 – 43	NGC5090	5.0x3.3(−26°)	0.70	1.58	0.90
1637 – 77		4.4x2.6(−87°)	0.49	1.18	0.45
1733 – 56		2.0x1.7(+68°)	0.70	2.30	0.68
		6.2x4.9(+86°)	1.60	–	–
1839 – 48		2.6x1.6(+48°)	0.36	1.15	0.90
2250 – 41		2.5x1.8(+16°)	1.10	1.12	0.86

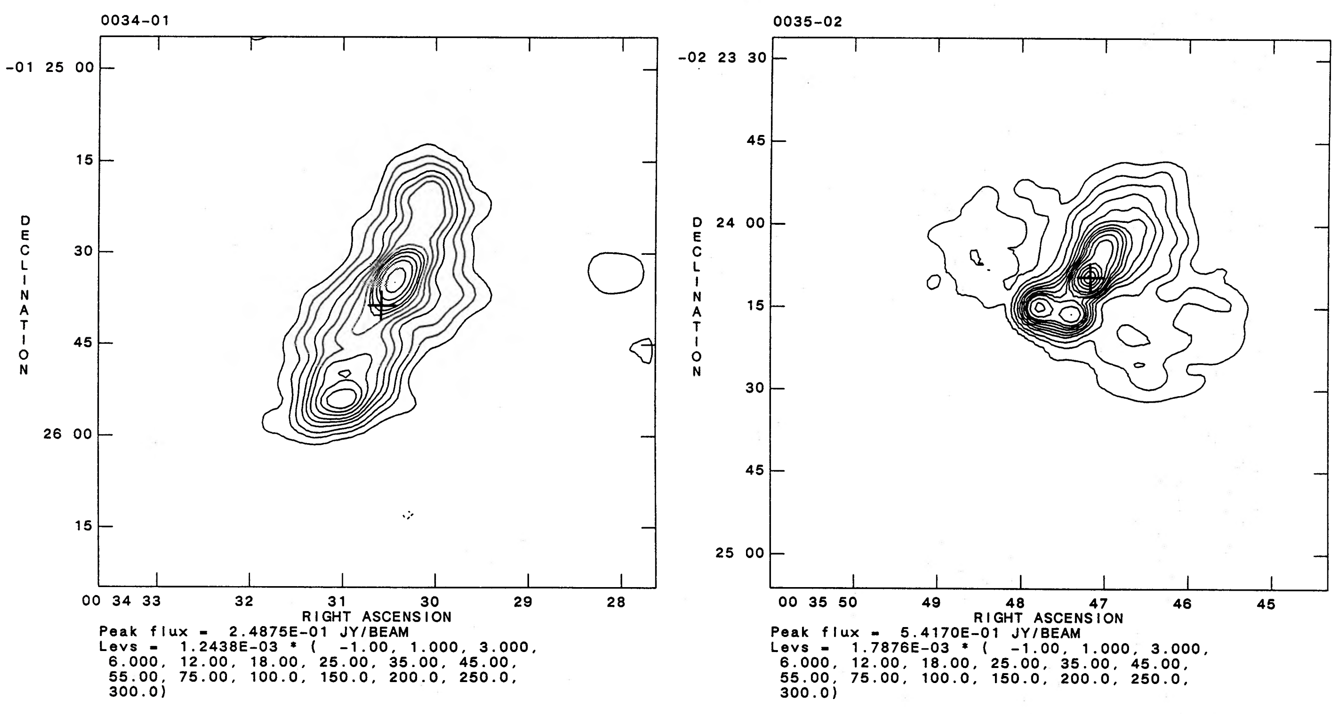

Figure 1. The VLA images of extended sources.

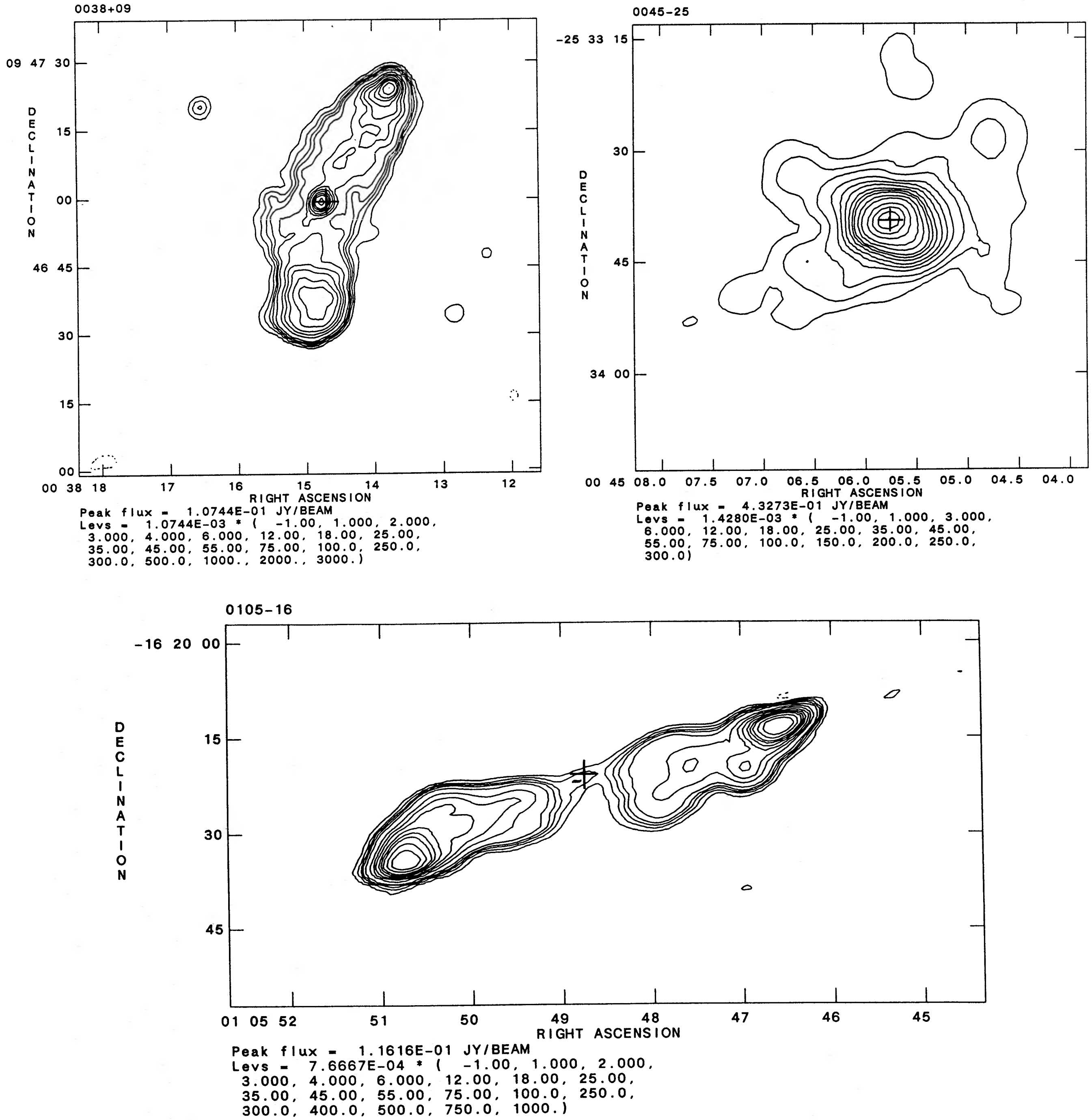

Figure 1 – *continued*

Section 4) and in Table 3 (see Section 3.4). We could find useful information for all but two of the remaining sources in the sample. These sources are 0039 − 44 and 1246 − 41, and they have been observed by Burgess (private communication) in a different ATCA project so that the data are not currently available to us.

3.4 Results of the VLA and ATCA data

Contour maps of our total intensity images for the VLA data are presented in Fig. 1 for the sources with extended structure. Similarly, the ATCA images are presented in Fig. 2. In both figures the crosses represent the optical position of the galaxy or quasar. In most cases this position coincides very well with the position of the radio core.

In Table 3 we show the radio parameters, obtained from the VLA and ATCA observations or collected from the literature, for 107 objects from the initial sample. In the table we list the 4.8-GHz total flux density (S_{tot} from WP85), the core (if present) flux density, the R parameter [$R = S_{core}/(S_{tot} - S_{core})$], the spectral index (from WP85), the total and core powers, and a morphological classification. For the

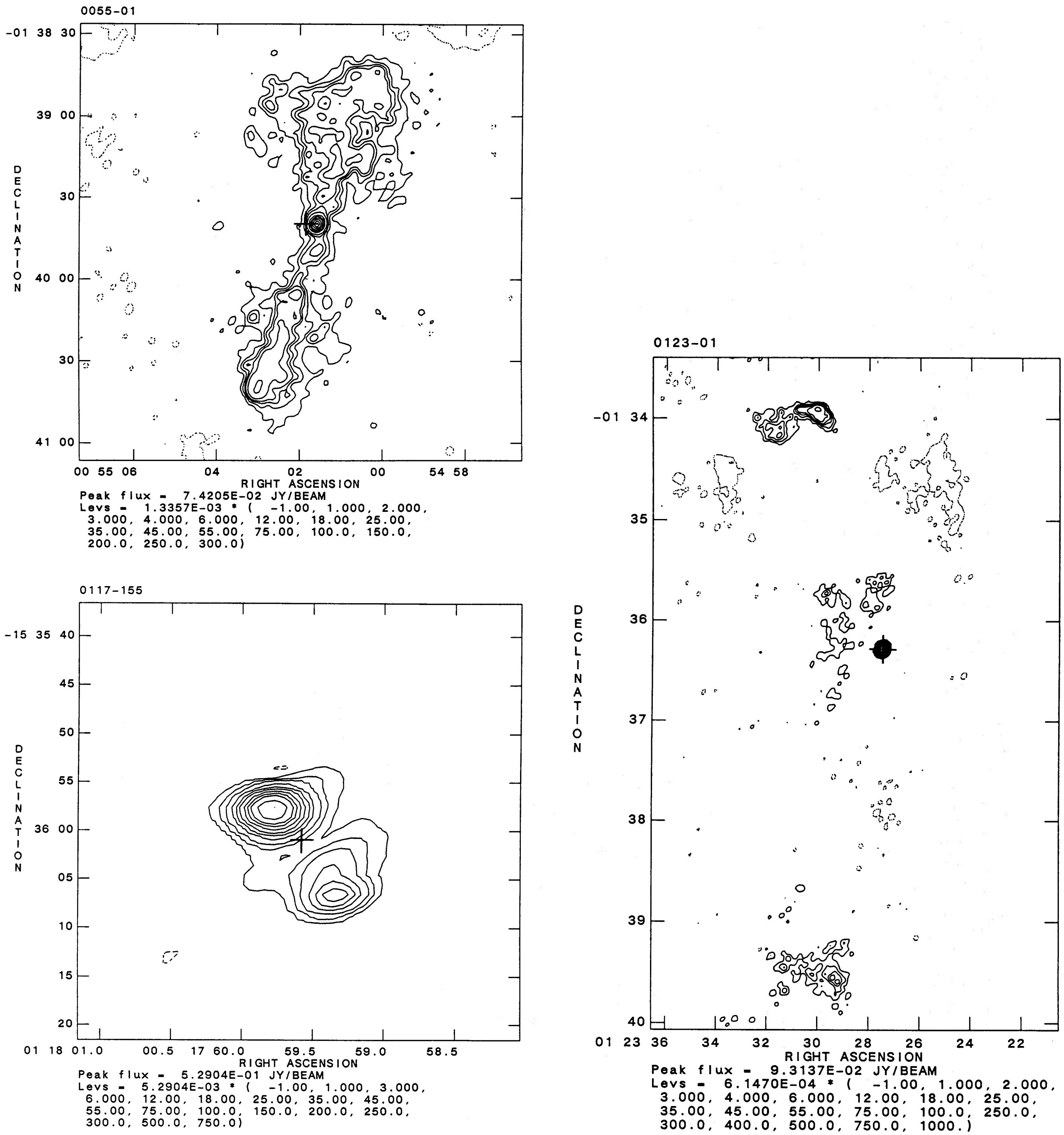

Figure 1 – *continued*

data taken from the literature the references are listed in the last column. For the unresolved objects we could not estimate a value for the R parameter; in those cases the symbol $\gg$ indicates that these objects are characterized by a large value of R. In a few cases, a better measurement of the radio core is present in the literature for some of the sources that we observed with the VLA; in these cases the value from the literature was taken and the reference is given in the table.

As previously mentioned, the relatively high resolution of the observations, coupled with the poor *uv* coverage, has the consequence that the extended structure is often poorly represented. This is illustrated in Fig. 3, where the VLA flux density is plotted against the 'total power' (WP85) flux density. The line indicates the ideal situation of equal flux density in both measurements. Some objects lie significantly below this line (the worst case is 0123−01, already clear from the radio map in Fig. 1). The few objects that are slightly above the line are all unresolved objects, and variability is the most likely explanation for the discrepancy. Since the percentage of flux density lost can be quite high in

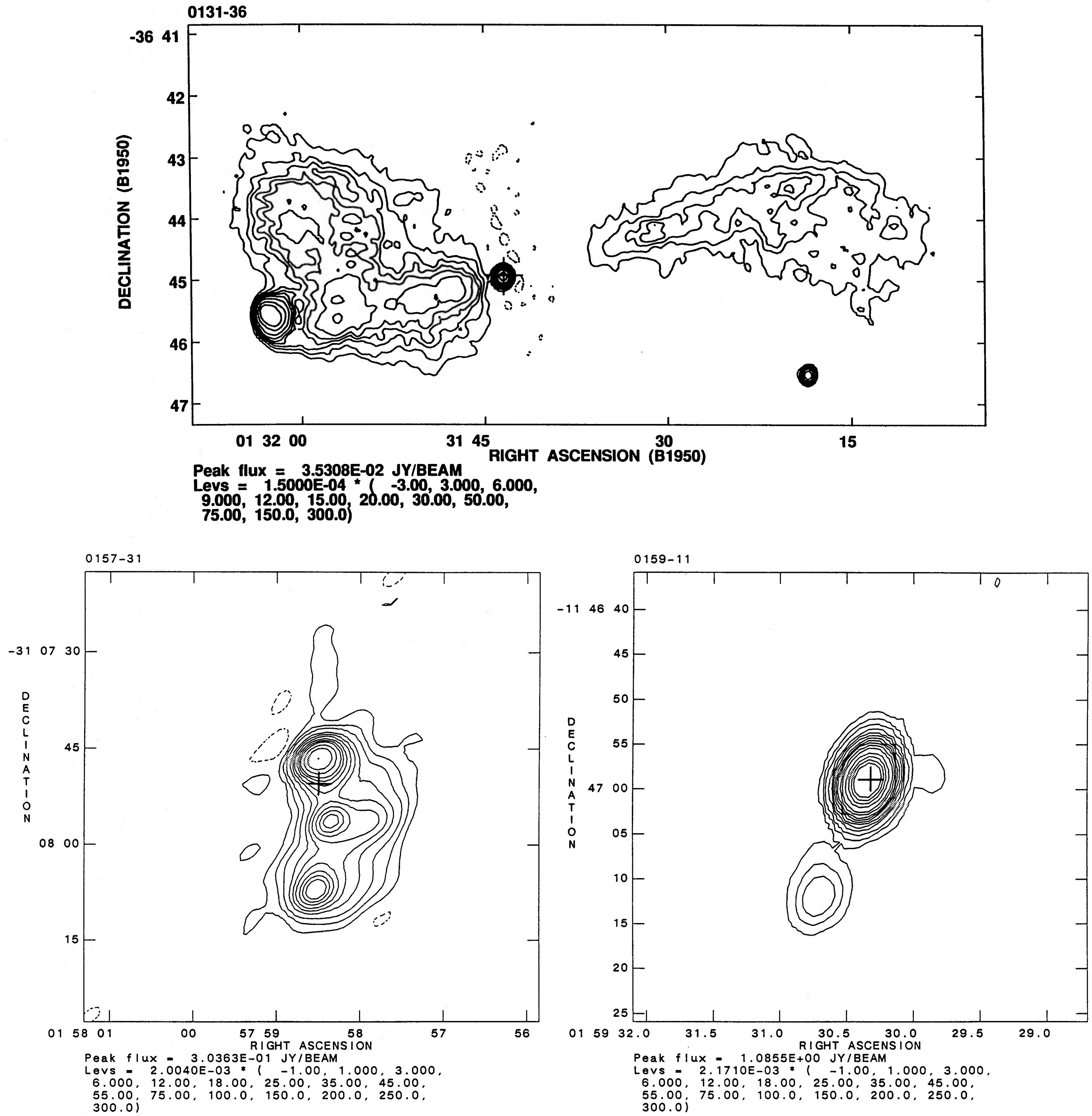

Figure 1 – *continued*

some cases, we use the 'total power' measurements for the correlations that use the total radio power (see Paper IV).

The positions of the radio cores (if present) were also measured for the observed objects (VLA and ATCA). These positions are listed in Table 4. For the sources in the 'complete sample', the agreement (within the errors) between the radio core position and the optical positions was verified. For the objects in the 'complete sample' without a radio core, the position of the optical identification is given in table 2 of Paper I. For the objects with $z > 0.7$, the optical solutions (and a discussion about the new identifications) are given in Paper III.

4 NOTES ON INDIVIDUAL SOURCES

Here we make some brief comments on the sources listed in Table 3 (either observed by us or collected from literature). A flag following the name of the object indicates that a contour plot of the source itself can be found either in Fig. 1 (*, VLA data) or in Fig. 2 (†, ATCA data).

0035 − 02* (3C 17). Our VLA image shows a triple source, or possibly an FR II adjacent to an FR I. The brightest component (which would be the core of the FR I) is very close to the optical position.

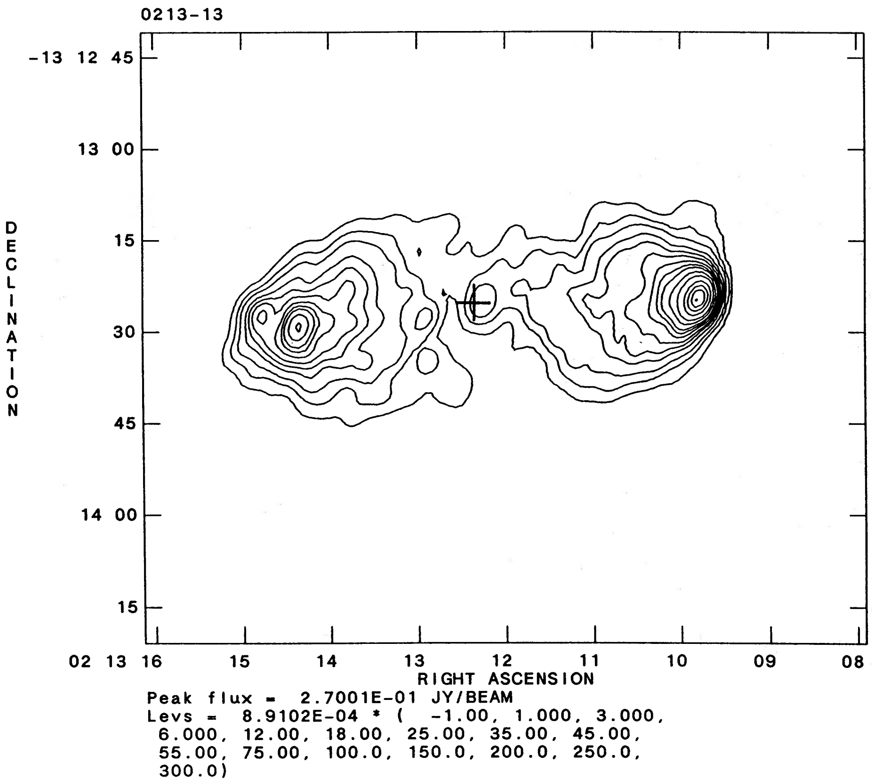

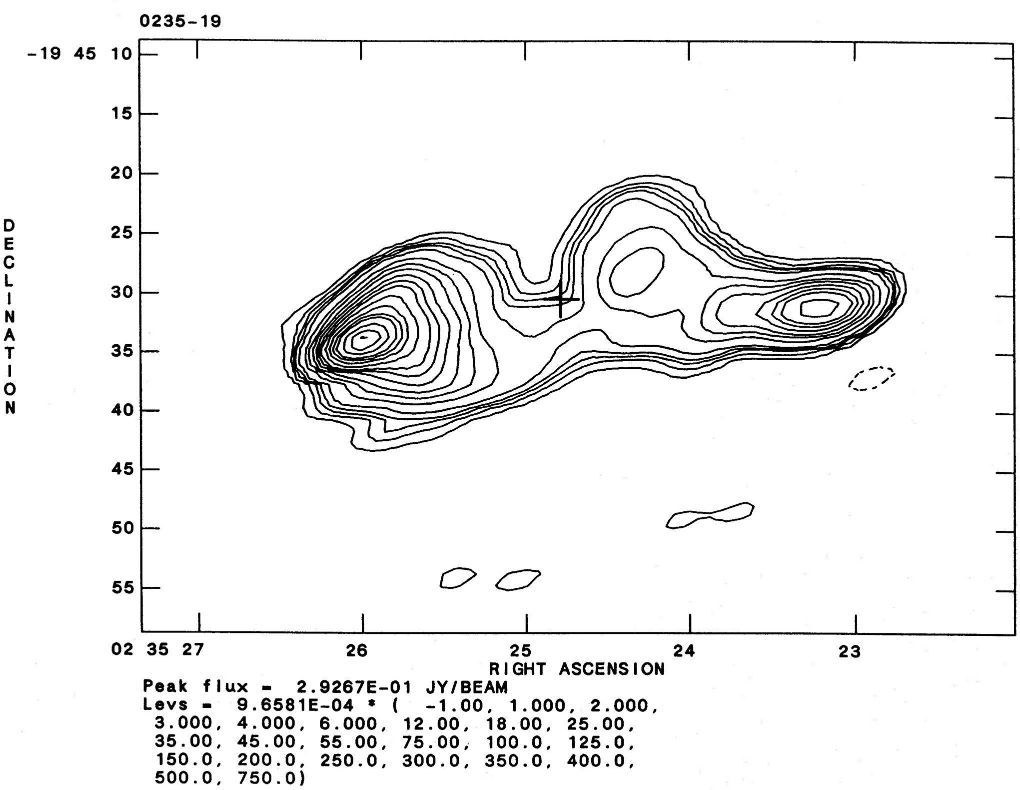

Figure 1 – *continued*

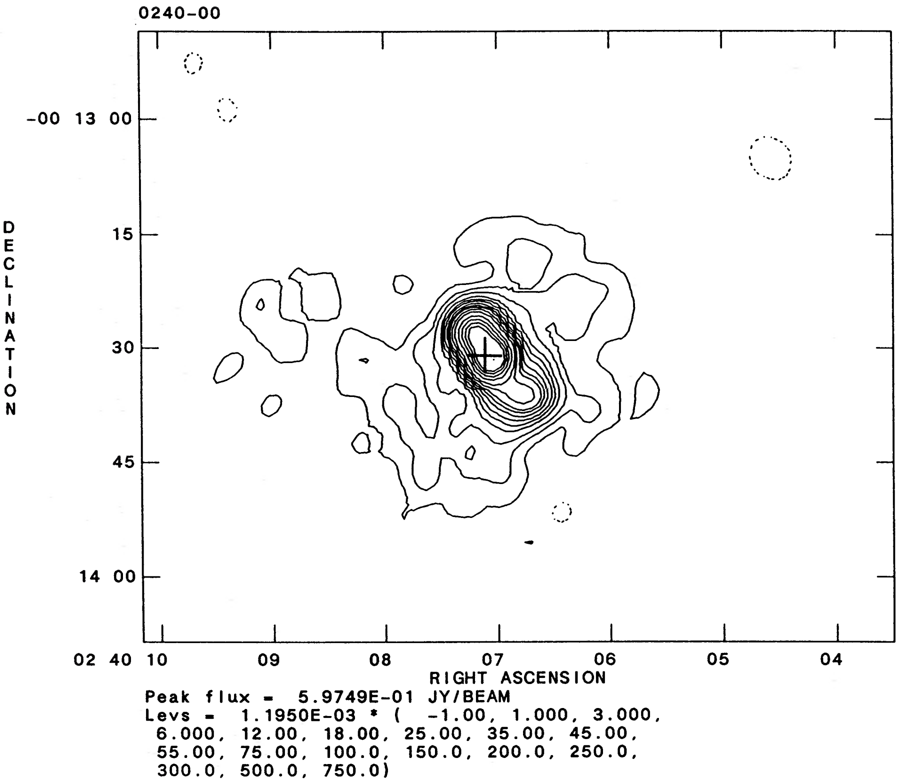

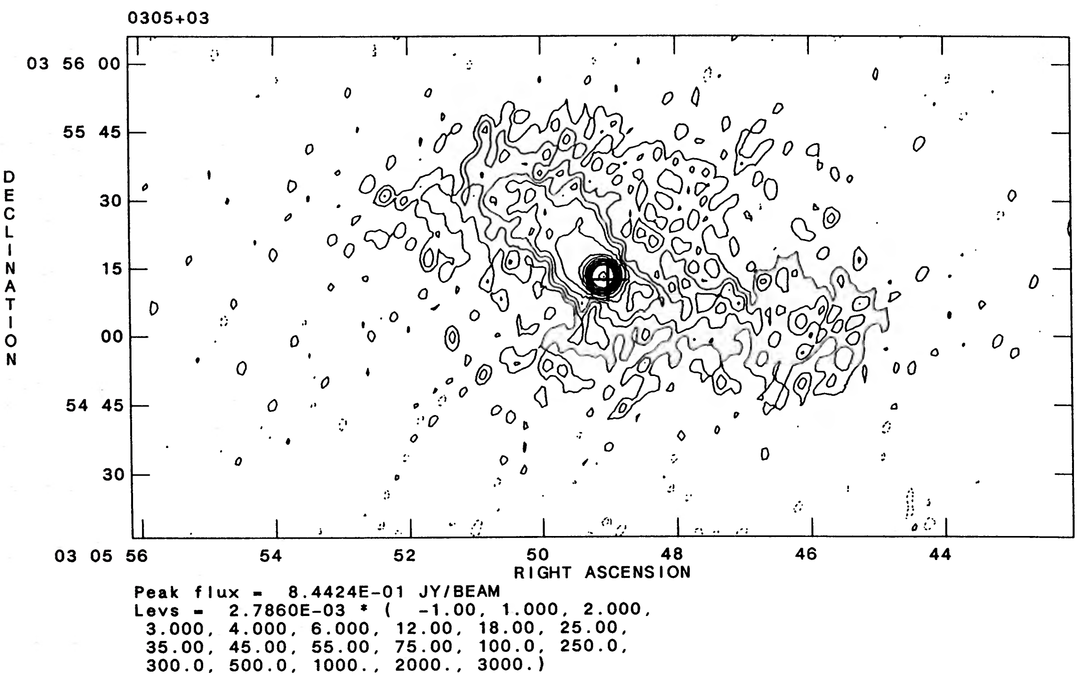

Figure 1 – *continued*

0043 − 42. At 6 cm and 4-arcsec resolution this FR II radio galaxy has no detected core and is dominated by the hotspots in the lobes (Duncan & Sproats 1992) which are separated by ~2.5 arcmin. Bridging emission extends from the hotspots to their mid-point. A low-resolution map obtained with MOST at 843 MHz was also secured by Jones & McAdam (1992).

0045 − 25* (NGC 253). A bright nearby spiral galaxy which is nearly edge-on (Ulrich 1978). The core measurement was taken from Ekers et al. (1989) rather than our own image, because their resolution was higher.

0014 − 21. This CSS source is unresolved at the resolution of our VLA observations; it is variable at low radio frequencies (Mantovani et al. 1992).

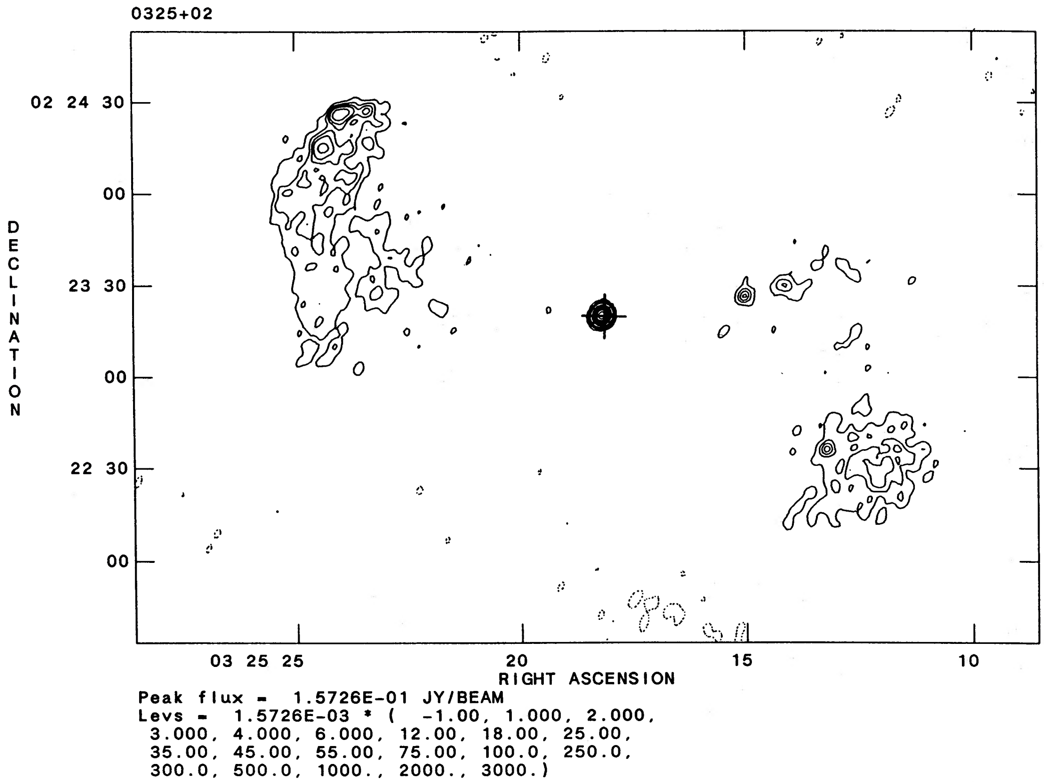

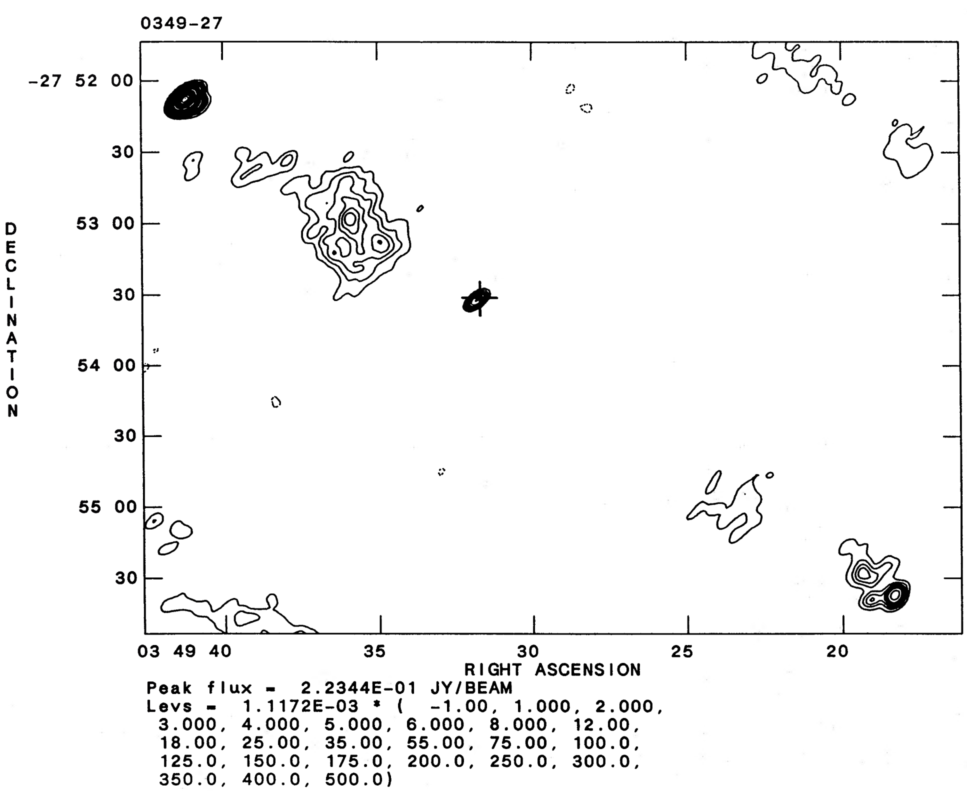

Figure 1 – *continued*

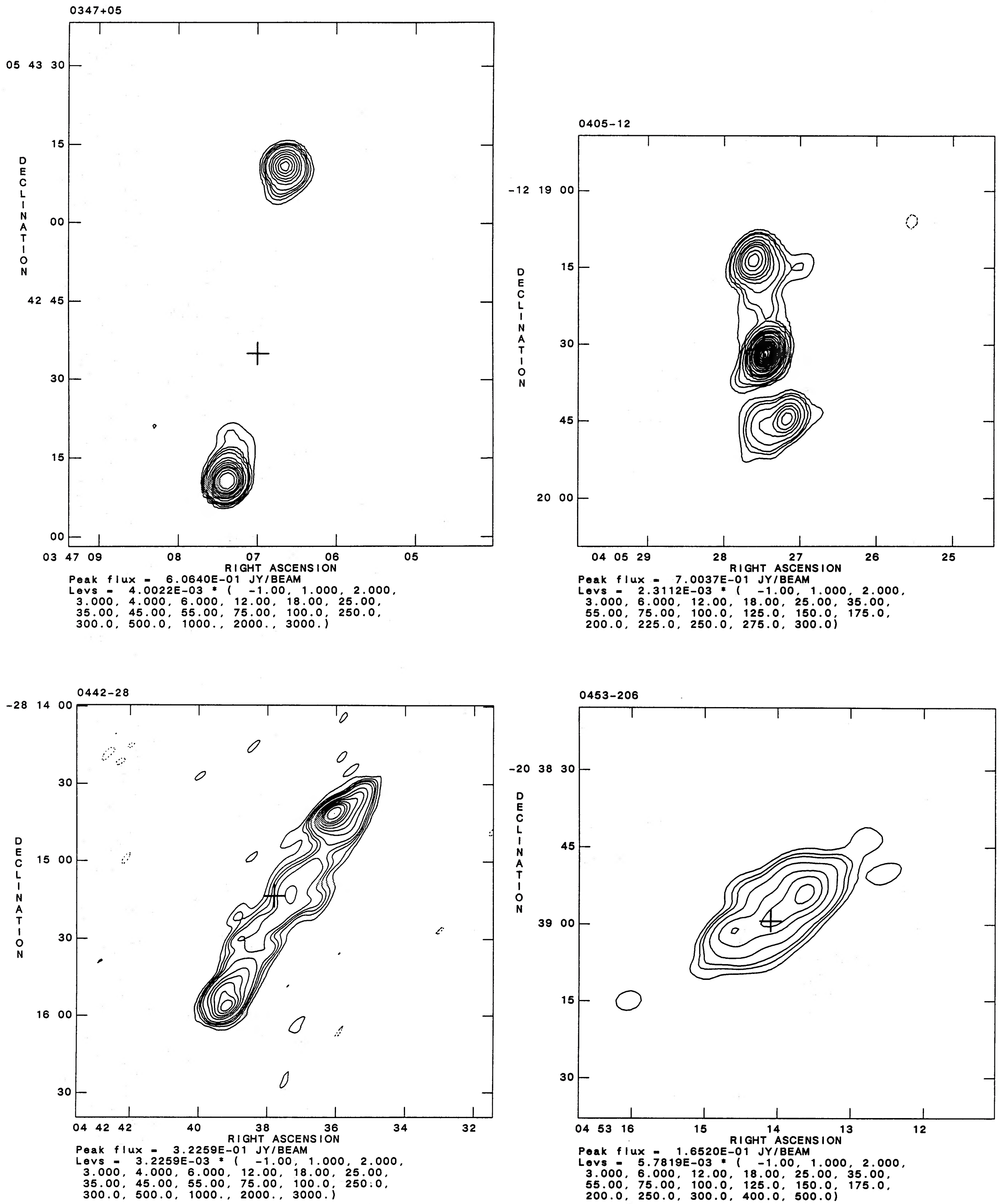

Figure 1 – *continued*

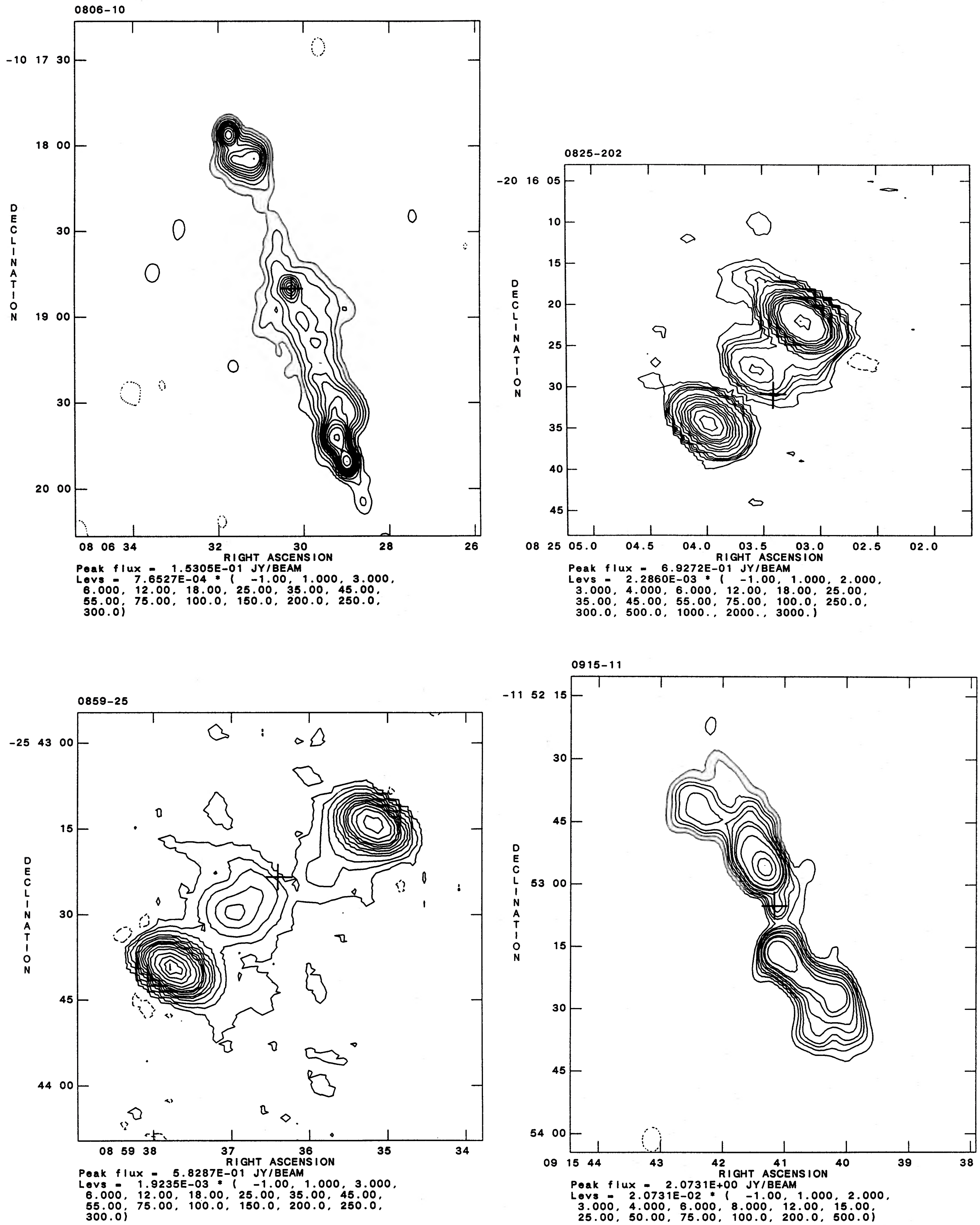

Figure 1 – *continued*

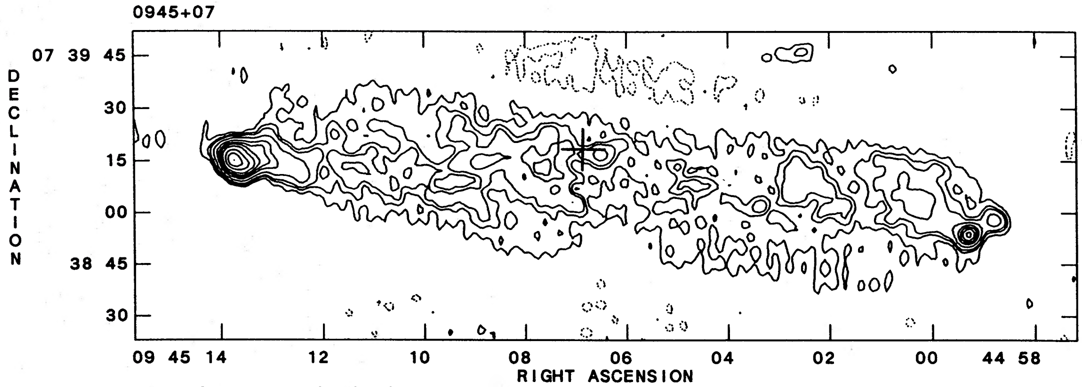

Peak flux = 1.6120E-01 JY/BEAM
Levs = 1.6120E-03 * (-1.00, 1.000, 2.000, 3.000, 6.000, 12.00, 18.00, 25.00, 35.00, 55.00, 75.00, 100.0, 125.0, 150.0, 175.0, 200.0, 250.0, 300.0, 400.0, 500.0)

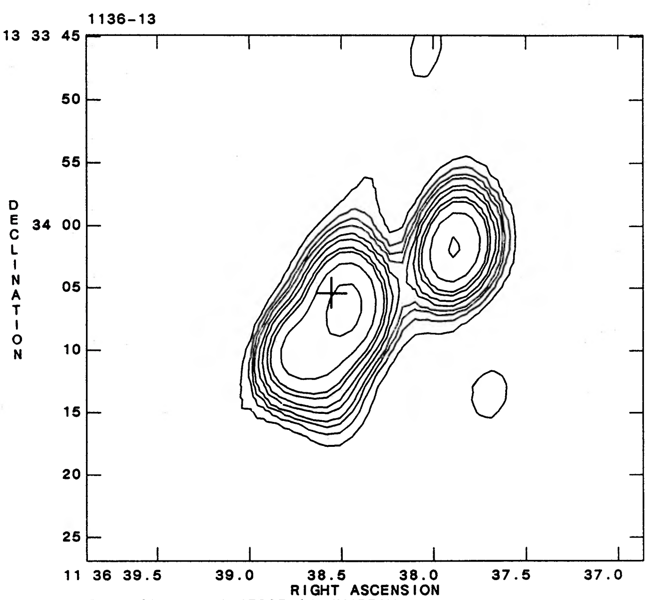

Peak flux = 4.4700E-01 JY/BEAM
Levs = 6.7051E-03 * (-1.00, 1.000, 2.000, 3.000, 4.000, 6.000, 8.000, 12.00, 15.00, 25.00, 50.00, 75.00, 100.0, 200.0, 500.0)

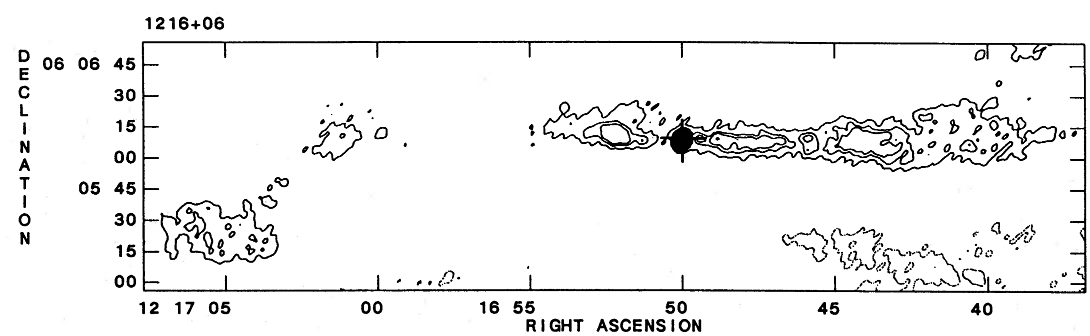

Peak flux = 2.8657E-01 JY/BEAM
Levs = 1.4328E-03 * (-1.00, 1.000, 2.000, 3.000, 6.000, 12.00, 18.00, 25.00, 35.00, 55.00, 75.00, 100.0, 125.0, 150.0, 175.0, 200.0, 225.0, 250.0, 275.0, 300.0)

Figure 1 – *continued*

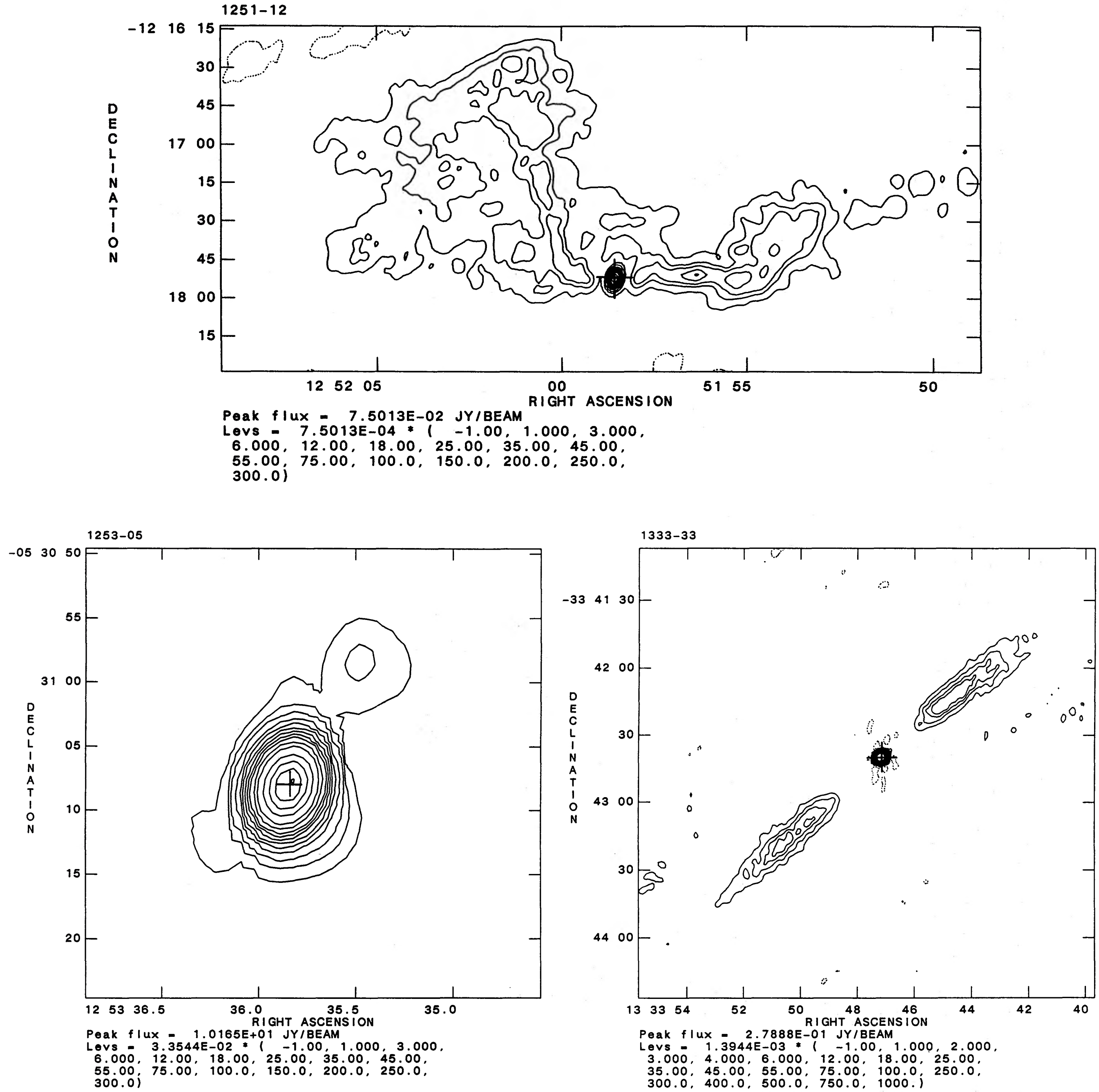

Figure 1 – *continued*

0131 – 36* (NGC 612). This is a very unusual S0 galaxy with a dust lane, a prominent stellar bulge, extended emission lines and a radio structure which our VLA image shows is FR II-like; it has a weak core and a bright hotspot in the eastern lobe. The contour representation of the emission masks the knotty jet leading to the eastern hotspot (it is apparent in grey-scale representations). The western lobe is much more diffuse.

0157 – 31*. A probable FR II quasar.

0159 – 11* (3C 57). A probable CSS quasar; there is possibly some extended emission adjoining the core in the VLA image.

0235 – 19*. The source is variable at low radio frequencies (Mantovani et al. 1992).

0240 – 00* (NGC 1068). A well-known Seyfert galaxy. Our VLA image shows a diffuse halo surrounding a bright component with a southern extension.

0255 + 05 (3C 75). This object is a pair of wide-angle-tail radio sources already observed by Owen et al. (1985). Baum et al. (1988) present an image of the Hα + [N II] emission of this object.

0305 + 03* (3C 78). This is an S0 galaxy. From our VLA observation the core is well resolved, while part of the extended structure is lost.

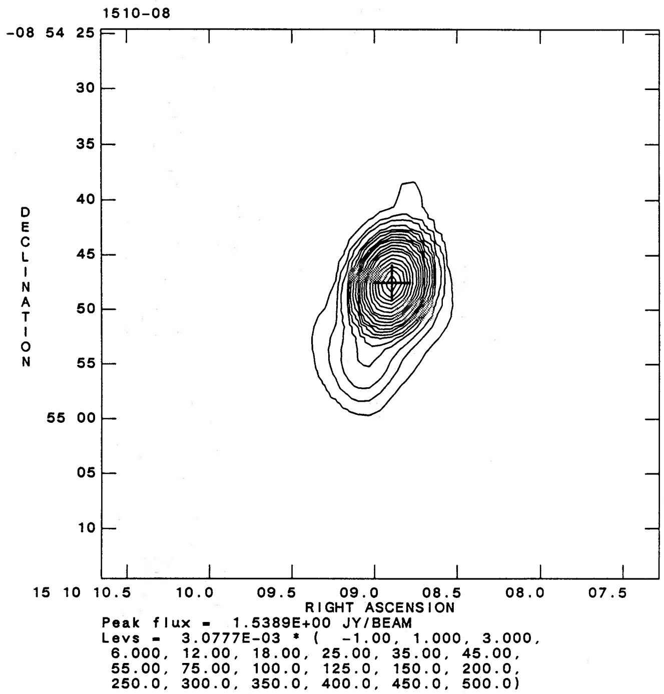

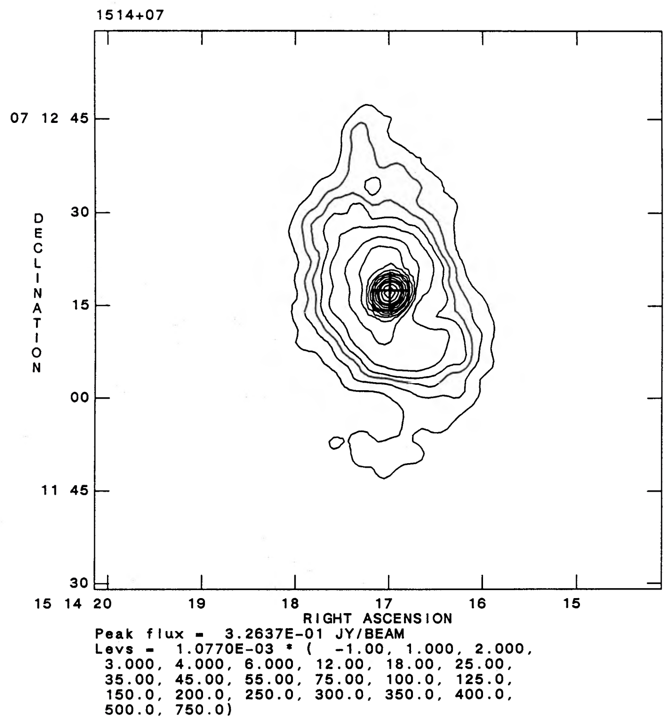

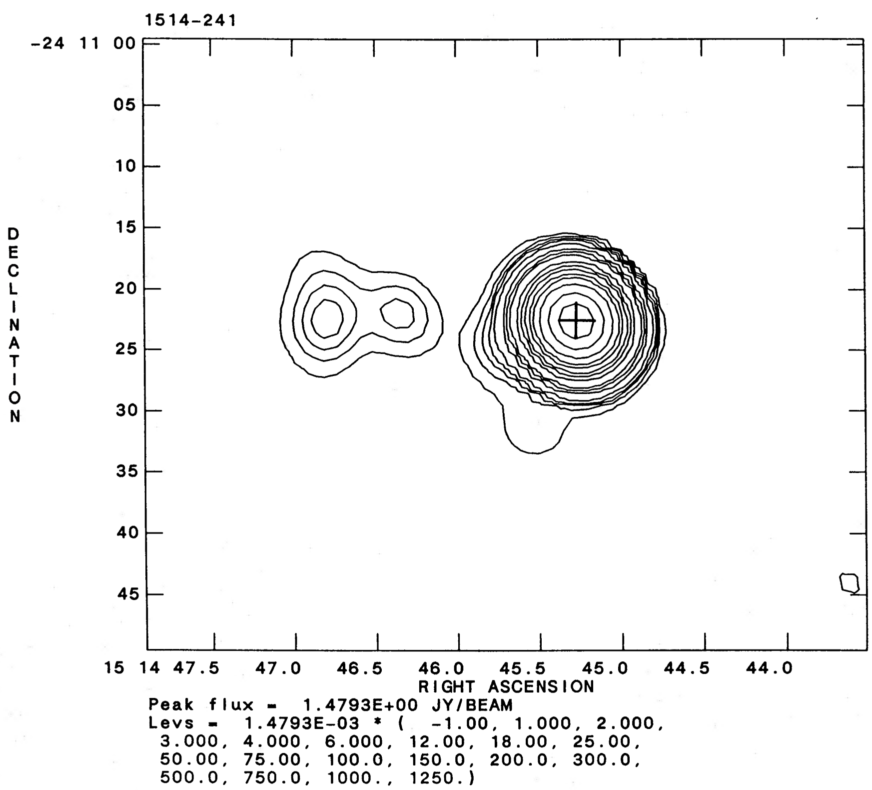

Figure 1 – *continued*

0320 − 37 (For A). One of the closest and most famous sources in the Southern Hemisphere. The radio image shows two 'flat', low-brightness lobes and a weak core in the middle. These lobes are extremely filamentary at high resolution. It is presumably an FR I, but not very typical.

0325 + 02* (3C 88). An FR II radio galaxy; a large part of the faint diffuse emission is lost in our VLA image, but the core is evident. A better lower resolution contour map that shows the overall structure is in Baum et al. (1988) together with an Hα + [N II] image.

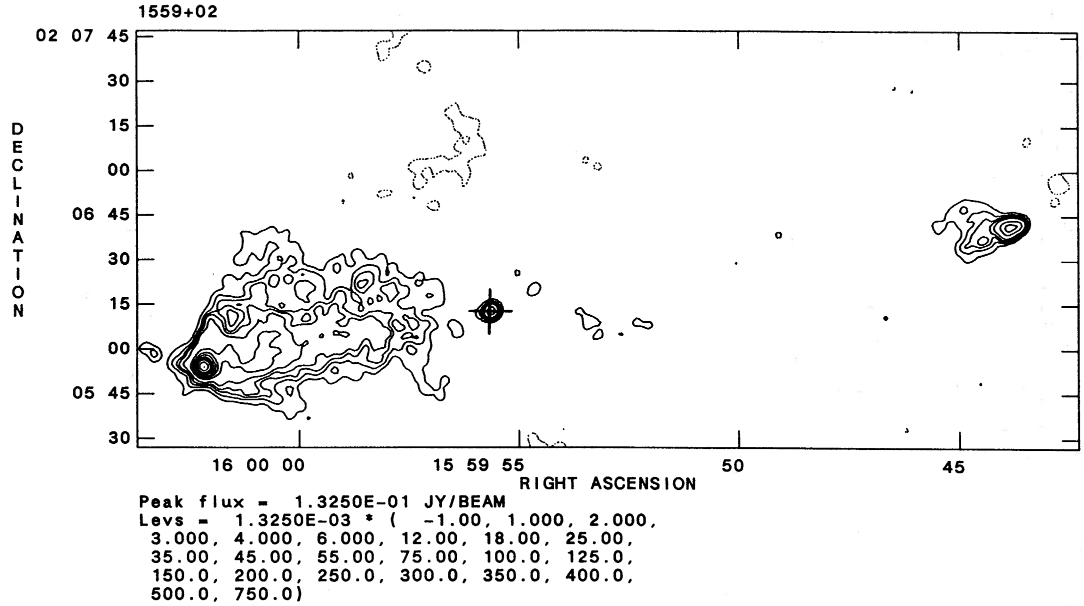

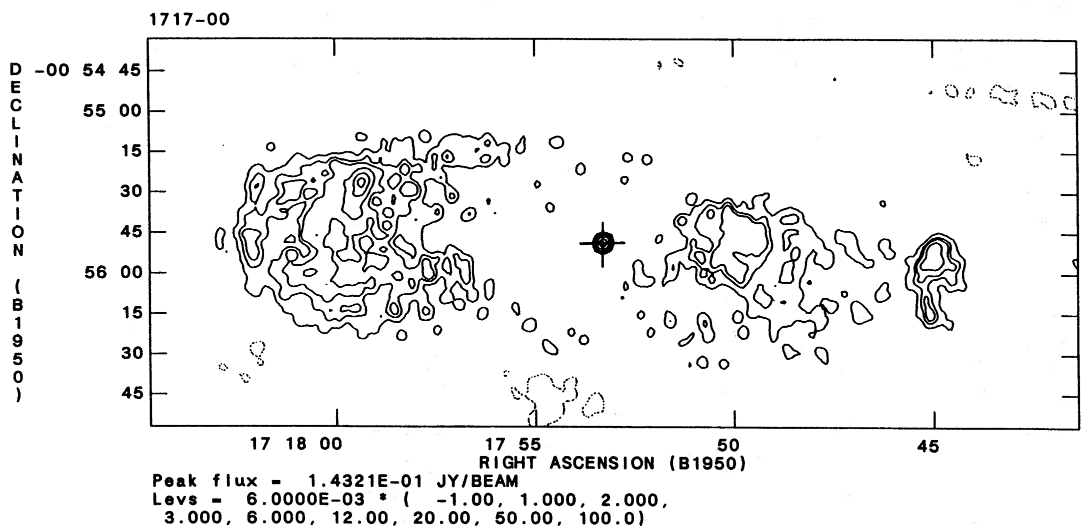

Figure 1 – *continued*

0349 − 27*. A well-known FR II radio galaxy. A detailed optical study is presented by Danziger et al. (1984). The optical galaxy has extended emission-line regions.

0407 − 65. This compact source is classified as GPS (GHz peaked source) by O'Dea, Baum & Stanghellini (1991).

0427 − 53†. An interesting radio galaxy with a long tongue of emission, seen extending westward from the western lobe in the 843-MHz Molonglo image (Jones & McAdam 1992). Our ATCA image shows only the inner lobes and a distinct core. The extended emission in this image is not reliably represented. This source is probably an FR II.

0430 + 05 (3C 120). This Seyfert galaxy has been exhaustively studied at a variety of resolutions (see Walker, Benson & Unwin 1987). It has structure on scales from 100 kpc to 1 pc, including a prominent one-sided jet.

0453 − 20*. This galaxy has diffuse and amorphous radio emission. Our VLA image does not show an obvious core at the optical position.

0500 + 01. O'Dea, Baum & Stanghellini (1991) classified this compact source as GPS.

0625 − 53. This FR I radio galaxy was observed by Duncan & Sproats (1992). They find a core and distorted diffuse lobes. The position of the core coincides with the eastern galaxy of a dumbbell system (Paper I).

0806 − 10*. Our spectrum, from which a new redshift was measured (see Paper I), shows extended emission lines.

0945 + 07* (3C 277). An FR II radio galaxy. In the radio contour map presented by Baum et al. (1988) the low-brightness lobes are more visible. This object contains extensive emission-line regions (Baum et al. 1988; Prieto et al. 1993).

1216 + 06* (3C 270). An FR I radio galaxy with a two-sided jet emanating from a bright core in our VLA image, and large symmetric lobes (Prestage 1985).

1245 − 19. A CSS radio galaxy found to be variable at low frequencies (Mantovani et al. 1992).

1251 − 12* (3C 278). This FR I radio galaxy is a wide-angle-tail source; this is clearer in the image presented by

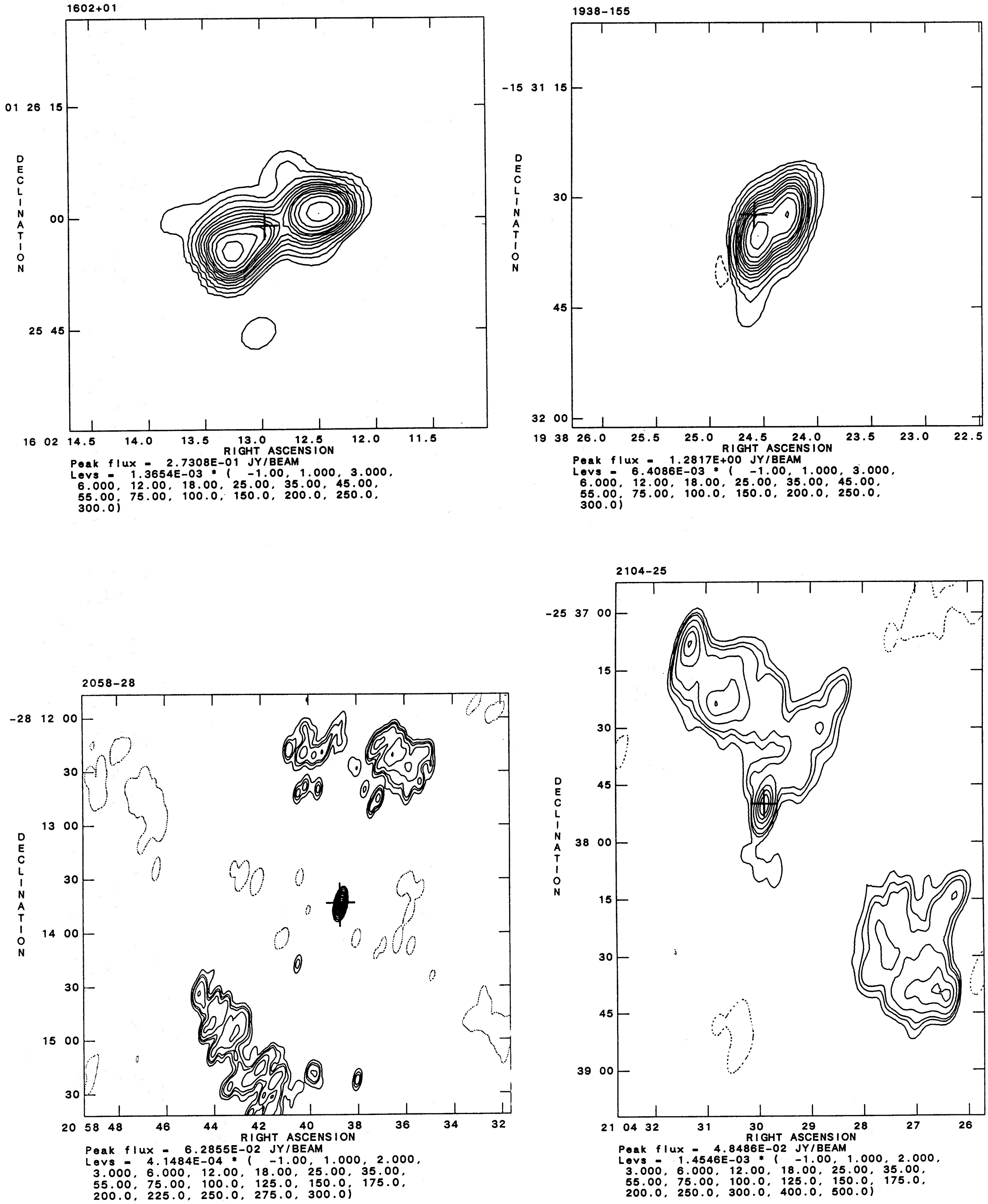

Figure 1 – *continued*

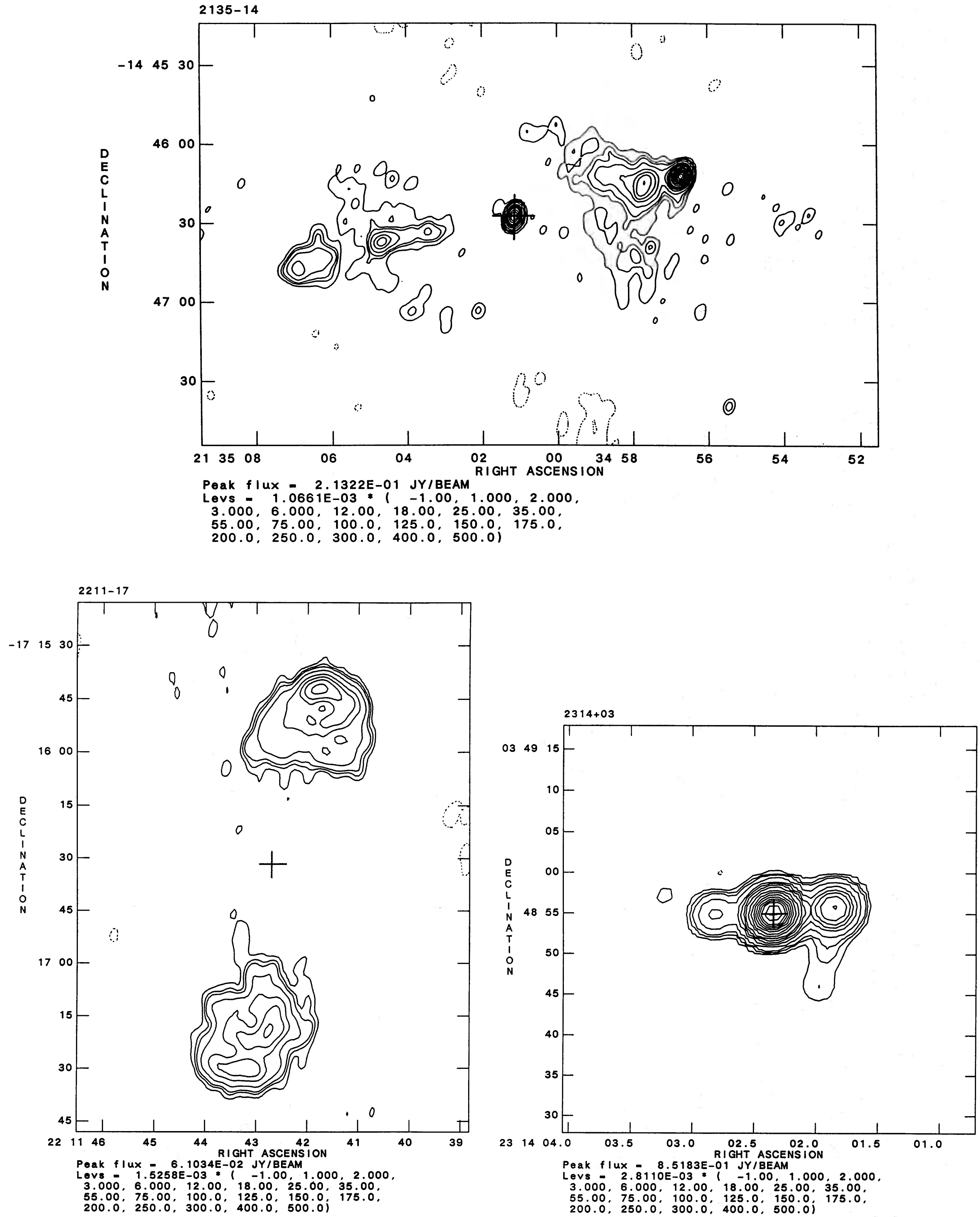

Figure 1 – *continued*

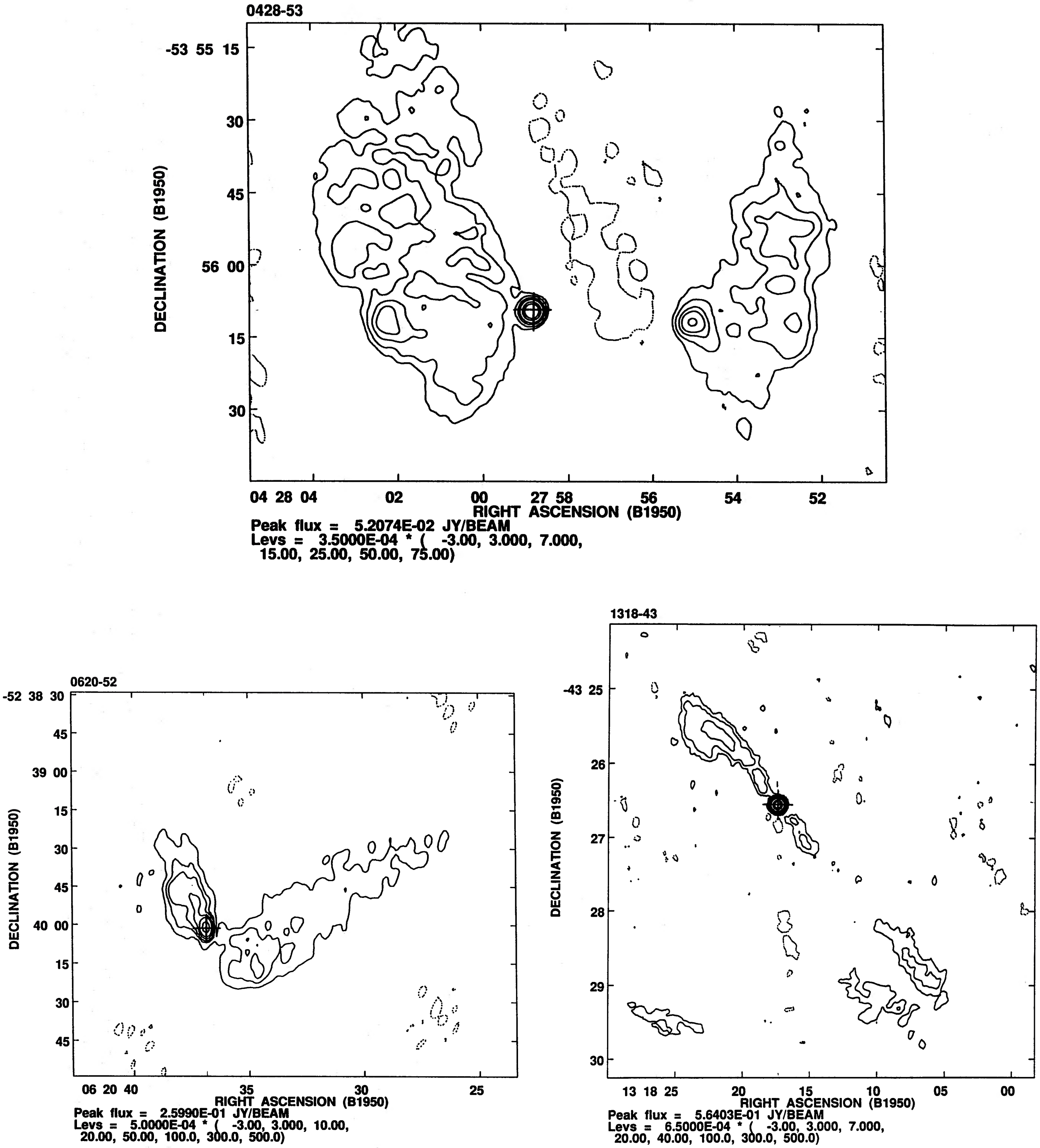

Figure 2. The ATCA images of extended sources.

Baum et al. than in our VLA image. Baum et al. (1988) also show an Hα + [N II] image.

1318 − 43† (NGC 5090). An FR I radio galaxy; our ATCA image shows a core, asymmetric two-sided jet and diffuse lobes. The lobes are poorly represented in this image. The 843-MHz MOST image (Jones & McAdam 1992) shows that emission trails away from both lobes over several arcmin.

1333 − 33* (IC 4296). This radio galaxy has aspects of both FR I and FR II: bright symmetric jets but lobes with 'warm' rather than 'hot' spots.

1514 + 07* (3C 317). This radio galaxy is shown by our VLA image to have an unusual asymmetric core–halo-type structure. Baum et al. (1988) also show an Hα + [N II] map.

1514 − 24* (Ap Lib). A well-known BL Lac object observed by Conway & Stannard (1972) and by Ekers et al.

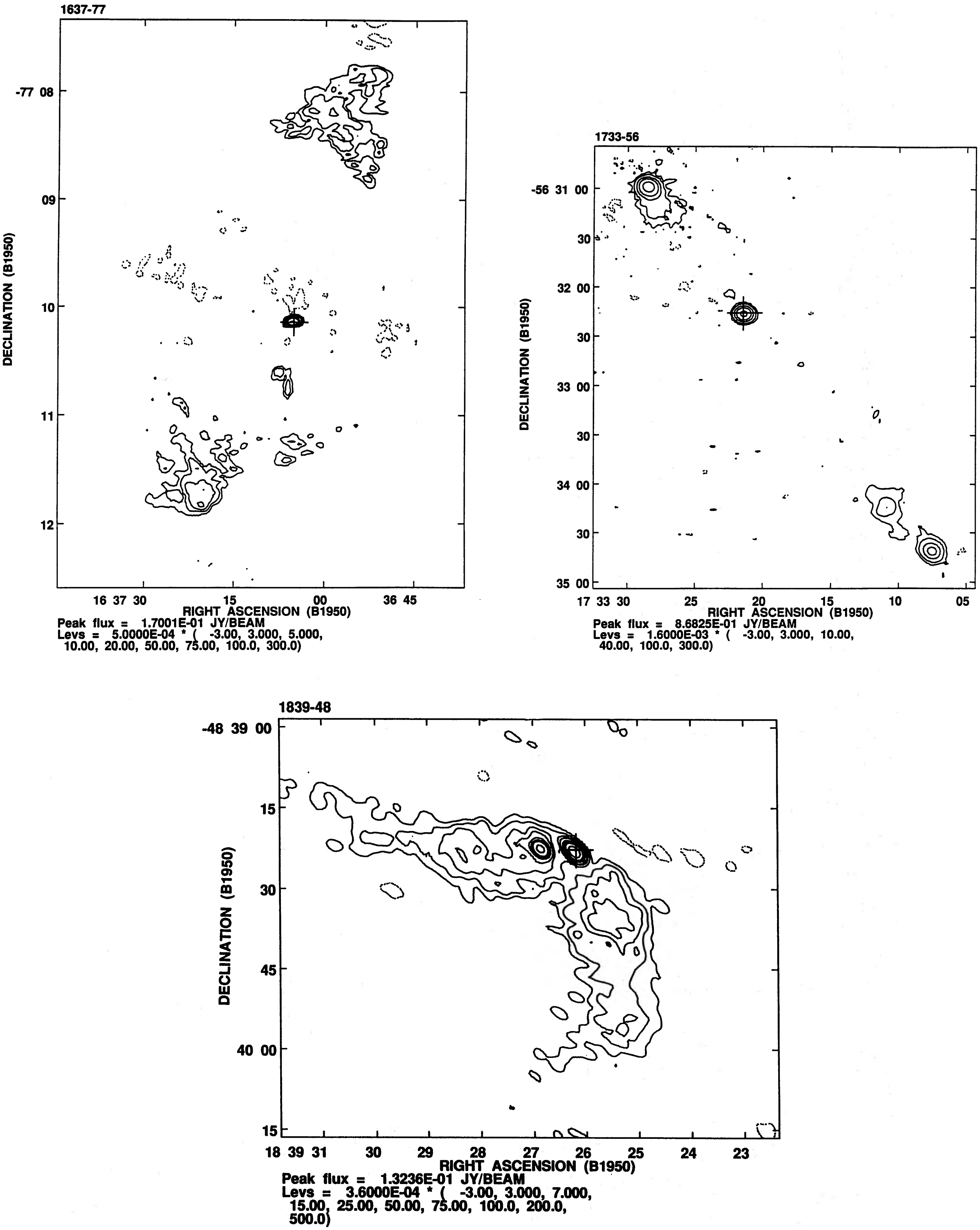

Figure 2 – *continued*

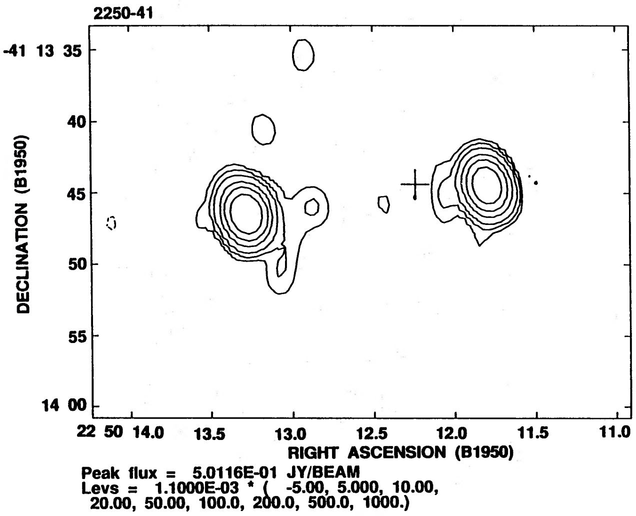

Figure 2 – *continued*

(1989). Our VLA measurement of the radio core agrees very well with the high-resolution measurement given in the former paper.

1559 + 02* (3C 327). In Baum et al. (1988) one can see that the emission from the more distant lobe also extends back to the core. They also show an Hα + [N II] image.

1637 − 77†. An FR II radio galaxy. Our ATCA image represents the extended structure poorly, but the main features are reliable. Only the southern lobe contains what would be termed a hotspot.

1648 + 05 (Her A). A very well-known and unusual radio galaxy (presumably an FR I) studied by Dreher & Feigelson (1984). We took the core flux density from Feigelson (private communication).

1717 − 00* (3C 353). This FR II radio galaxy has an extended low-brightness halo (Baum et al. 1988) which is resolved out in our VLA image.

1733 − 56†. An FR II radio galaxy; our ATCA image does not show all the extended structure, but shows the compact hotspots and core.

Table 3. 2-Jy sample – the radio parameters.

Object	Other Name	S_{tot} Jy	S_{core} Jy	R	$\alpha_{2.7}^{4.8}$	log P_{tot} W/Hz	log P_{core} W/Hz	Morph.	Ref.
0008−42*		1.34	–	>>	1.04	28.70†	–	U	1
0022−42*		1.79	–	>>	0.77	27.73†	–	U	1
0023−26	OB-238	3.41	–	>>	0.70	27.29	–	U	
0034−01	3C15	1.60	0.299	0.230	0.79	25.59	24.87	II	
0035−02	3C17	2.64	0.662	0.335	0.72	26.81	26.21		
0038+09	3C18	1.66	0.083	0.053	1.00	26.49	25.18	II	
0043−42		2.98	<0.006	<0.002	0.87	26.28	<23.59	II	2,7
0045−25	NGC253	2.44	0.130[a]	0.056	0.62	22.03	20.75	core/halo	3
0055−01	3C29	2.20	0.093	0.044	0.76	25.30	23.93	I	4
0105−16	3C32	1.17	<0.002	<0.002	1.10	27.08	<24.32	II	
0114−21*	OC-224	1.27	–	>>	0.95	28.64†	–	U	
0117−15	3C38	1.60			0.90	27.54		II	
0123−01	3C40	1.88	0.100	0.056	0.91	24.43	23.16	II	32
0131−36	NGC612	4.08	0.038	0.009	0.51	25.21	23.18	II	3,22,23
0157−31*	OC-397	1.47	0.070	0.050	0.81	28.94†	28.62†	II	
0159−11	3C57	1.37	–	–	0.64	27.60	–		
0213−13	3C62	1.80	0.024	0.014	0.74	26.28	24.41	II	
0235−19	OD-159	1.44	<0.0002[c]	<0.0001	0.87	27.59	<23.73	II	
0240−00	NGC1068	1.98	0.075[b]	0.040	0.78	23.14	21.72		
0252−71		1.58	–	>>	1.14	27.58	–	U	1
0255+05	3C75	1.98	0.039	0.020	0.86	24.67	22.96	I	4,5
0305+03	3C78	3.65	0.964	0.359	0.64	25.13	24.56	I	4,24,25
0320−37	For A	72.00	0.026	0.0004	0.52	24.89	21.45	I	3,6,7,26
0325+02	3C88	1.99	0.159	0.087	0.79	24.90	23.80	II	
0347+05*	4C05.16	1.26	<0.0015	<0.0012	0.78	27.73	<24.80	II	
0349−27	OE-283	2.04	0.013	0.006	0.59	25.60	23.41	II	3,4,27
0403−13	OF-105	3.25	–	>>	−0.05	27.68	–	U	
0404+03	3C105	2.39	0.014	0.0059	0.60	25.94	23.71	II	4
0405−12	OF-109	1.83	0.760	0.710	0.42	27.52	27.14	II	
0407−65*		3.36	–	>>	1.11	28.39†	–	U	1
0409−75		4.25			0.86	28.17		II	2
0427−53		3.41	0.057	0.017	0.20	25.33	23.56	I?	
0430+05	3C120	8.60	3.458	0.67	−1.71	25.59	25.19		8
0442−28	OF-271	2.21			0.93	26.38	–	II	
0453−20	OF-289	1.81	0.04[a]	0.023	0.73	25.00	23.34	I?	3

Table 3 – *continued*

Object	Other Name	S_{tot} Jy	S_{core} Jy	R	$\alpha_{2.7}^{4.8}$	log P_{tot} W/Hz	log P_{core} W/Hz	Morph.	Ref.
0500+01*	OG3	1.87	–	>>	0.47	28.09†	–	U	
0518–45	Pic A	15.37	1.0^f	0.070	1.07	25.93	24.74	II	7,9,27
0521–36		9.35	1.400	0.176	0.49	26.10	25.28		3,10,28
0605–08*	OH-10	3.36	–	>>	–0.37	27.99	–	U	
0620–52		1.25	0.260	0.263	0.87	25.17	24.49	I	7
0625–35		2.12	0.600	0.395	0.53	25.46	24.91	I	3,7
0625–53		1.85	0.042	0.023	1.17	25.40	23.75	II?	2
0637–75		5.45	–	>>	–0.32	27.96	–	U	11
0736+01	OI61	2.06	–	>>	0.18	26.53	–	U	
0743–67*		1.51			0.97	28.65			2
0806–10	3C195	1.63	0.055	0.035	0.72	25.97	24.50	II	
0825–20*	OJ-242	1.20	<0.046	<0.038	0.964	27.84	<26.42	II	
0834–19*	OJ-158.1	1.54	–	>>	0.82	28.16	–	U	
0842–75		1.40	0.59^e	0.728	0.72	27.37	27.00	core/jet	21
0858–27*	OJ-297	1.40	–	>>	0.60	28.89	–	U	
0859–25	OJ-299	1.74	<0.104	<0.064	1.08	26.98	<25.76	II	
0915–11	HydA	13.78	0.217^d	0.016	0.90	26.26	24.46	I	4,33
0945+07	3C227	2.64	0.032	0.0123	0.82	25.96	24.04	II	
1015–31*	OL-327	1.35	–	>>	0.84	27.43†	–	U	
1136–13	OM-161	1.90			0.65	27.55			
1151–34	OM-386	2.78	–	>>	0.69	26.98	–	U	
1216+06	3C270	9.18	0.308	0.0347	0.56	24.16	22.68	I	
1226+02	3C273	40.07	26.19	1.888	–0.05	27.64	27.45	core/jet	12,13
1245–19*	ON-176.2	2.51	–	>>	0.76	28.59	–	U	
1251–12	3C278	2.5	0.088	0.0365	0.93	24.40	22.94	I	
1253–05	3C279	15.89	11.580	2.69	–0.59	28.21	28.07		
1306–09	OP-10	1.90	–	>>	0.65	27.37	–	U	
1308–22*	3C283	1.12	–	>>	1.30	28.13†	–	U	
1318–43	NGC5090	1.75	0.58	0.50	0.96	23.97	23.49	I	
1322–42	Cen A	62.83	6.984	0.125	1.20	23.95	22.99	I	14,29
1333–33	IC4296	6.30	0.297	0.0495	0.79	24.67	23.35	I(II)	30,31
1355–41		1.44	0.037	0.026	0.93	26.91	25.32	II	2,7
1510–08	OR-107	3.24	1.613	0.913	–0.13	27.26	26.94		
1514+07	3C317	0.96	0.391	0.687	1.20	24.73	24.34	core/halo	
1514–24	ApLib	1.94	1.480	3.22	0.13	25.29	25.17	core/jet	
1518+04*	4C04.51	1.03	–	>>	1.28	28.41	–	U	
1547–79		1.38	<0.003^e	<0.002	0.85	27.31	<24.65	II	2,21
1549–79		4.47	–	>>	0.17	26.63	–	U	1
1559+02	3C327	2.87	0.028	0.0099	0.95	26.17	24.16	II	
1602+01	3C327.1	1.13	0.065^d	0.061	1.07	27.21	25.97	II	4
1622–25*	OS-237.8	2.03	–	>>	0.19	28.23†	–	U	
1637–77		2.61	0.184	0.0759	0.62	25.29	24.14	II	7
1648+05	Her A	12.74	0.01	0.0008	1.11	27.19	24.08	I(II)	15,16
1717–00	3C353	20.54	0.117	0.0057	0.84	25.95	23.82	II	
1733–56		3.37	0.68	0.253	0.73	26.18	25.48	II	7,27
1740–51*		3.00	–	>>	0.72	27.30†	–	U	1
1814–63		4.37	–	>>	0.92	25.90	–	U	1
1839–48		1.28	0.163	0.146	0.75	25.88	24.99	I	21
1932–46		3.47	<0.06	<0.017	1.03	27.01	<25.24	II?	2
1934–63		6.45	–	>>	0.88	27.05	–	U	1,17
1938–15	OV–164	2.34			0.82	27.47			
1949+02	3C403	2.39	0.01	0.0042	0.73	25.58	23.20	II	4
1954–55		2.31	0.050^e	0.020	0.78	25.62	23.91	I	7,21
1954–38		2.00	–	>>	0.00	27.56	–	U	1
2008–06*	OW-15	1.35	–	>>	0.82	28.12†	–	U	
2058–28		2.00	0.063	0.0325	0.74	25.11	23.61	I?	
2104–25	OX-208	4.31	0.058	0.0137	0.89	25.42	23.55	II	3,27
2128+04*	OX-208	2.07	–	>>	0.67	29.57†	–	U	

Table 3 – *continued*

Object	Other Name	S_{tot} Jy	S_{core} Jy	R	$\alpha_{2.7}^{4.8}$	log P_{tot} W/Hz	log P_{core} W/Hz	Morph.	Ref.
2128−12	OX-148	2.00	–	>>	0.00	27.36	–	U?	
2135−14	OX-158	1.38	0.121	0.096	0.63	26.43	25.38	II	
2135−20	OX-20	1.53	–	>>	0.63	27.59	–	U	
2150−52*		1.17	<0.007	<0.006	0.95	28.42†	<26.2†	II	2
2152−69		12.65	0.40	0.033	0.71	25.61	24.11	I	6,18
2203−18	OY-106	4.28	–	>>	0.33	27.95	–	U	
2211−17	3C444	2.14	<0.002	<0.0009	1.26	26.42	<23.39	II	
2221−02	3C445	2.28	0.086	0.039	0.70	25.53	24.10	II	19
2243−12		2.38	–	>>	0.23	27.69	–	U	
2250−41		1.27	<0.003	<0.0023	0.99	26.86	<24.22	II?	2
2314+03	3C459	1.33	1.130	5.65	0.97	26.54	26.46	II	
2331−41*		1.52	<0.015	<0.010	0.91	28.04	26.03	II	21
2345−16		3.49	–	>>	0.26	27.78	–	core dom.	
2356−61		4.56	0.035	0.0077	1.36	26.32	24.20	II	7,20

References to Table 3.
Radio structure: (1) Duncan (1992); (2) Duncan & Sproats (1992); (3) Ekers et al. (1989); (4) Baum et al. (1988); (5) Owen et al. (1985); (6) Ekers et al. (1983); (7) Jones & McAdam (1992); (8) Walker et al. (1987); (9) Perley R. (private communication); (10) Keel (1986); (11) Costa M. E. (private communication); (12) Bridle & Perley (1984); (13) Browne et al. (1982); (14) Burns et al. (1983); (15) Dreher & Feigelson (1984); (16) Feigelson E. D. (private communication); (17) Fosbury et al. (1987); (18) Fosbury et al. (1990); (19) Kronberg et al. (1986); (20) Koekemoer et al. (private communication); (21) Burgess & Hunstead (private communication); (22) Goss et al. (1980); (23) Ekers et al. (1978); (24) Unger et al. (1984); (25) Saikia et al. (1986); (26) Fomalont et al. (1989); (27) Christiansen et al. (1977); (28) Danziger et al. (1979); (29) Junkes et al. (1992); (30) Killeen et al. (1986); (31) Killeen & Bicknell (1988); (32) O'Dea & Owen (1985); (33) Taylor et al. (1990).
Core fluxes: (a) Ekers et al. (1989); (b) Ulvestad et al. (1987), 2 cm; (c) Mantovani et al. (1992); (d) Baum et al. (1988); (e) Burgess & Hunstead (private communication); (f) Perley (private communication).
† z from PW85; *objects outside the complete sample ($z > 0.7$).

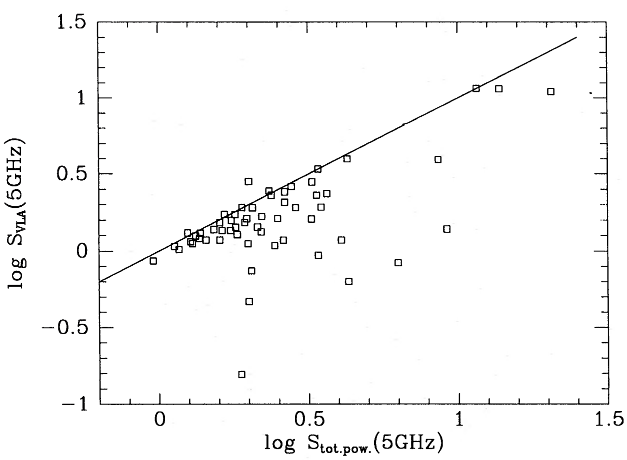

Figure 3. Logarithmic plot of the VLA flux density versus the 'total power' (WP85) flux density. The line indicates equal flux density in both measurements.

1839 − 487†. An FR I radio galaxy; our ATCA image shows a core and wide-angle tail-like emission trailing away. There is a compact component just to the east of the core. The low-resolution 843-MHz MOST image by Burgess & Hunstead (private communication) does not help to elucidate the nature of this source.

1954 − 55. This object was studied by Christiansen et al. (1977) and by Duncan & Sproats (1992). Its structure is hard to classify, but from the 843-MHz MOST image (Jones & McAdam 1992) it looks like an FR I. The Duncan & Sproats (1992) image shows a double structure, with the northern component slightly extended and brighter than the southern component.

2058 − 28*. This radio galaxy has very extended (11 arcmin) emission. It is probably an FR I. The best data at low resolution are in Christansen et al. (1977). At the higher resolution of our VLA image the majority of the extended structure is lost, but the radio core is well resolved and the brightest parts of the lobes are visible.

2135 − 14*. An FR II quasar; there is some suggestion of a jet towards the weaker hotspot.

2152 − 69. Fosbury et al. (1990) suggest that this radio galaxy is a blazar. The radio structure shows a core, a nearby bright lobe and a more distant diffuse lobe; in the true definition of Fanaroff & Riley, an FR II. There is a bright extended emission-line blob to the north-east of the core.

2250 − 41†. An FR II radio galaxy. The object also shows very extended emission lines in the same direction as the radio axis.

2356 − 61. An FR II radio galaxy imaged with the ATCA by Koekemoer et al. (private communication). The lobes have very compact hotspots with long bridges of emission extending back towards the weak core. Lower resolution

Table 4. Positions of the radio cores.

Object	Other Name	R.A. h m s	Dec. ° ′ ″
0023 − 26	OB-238	00 23 18.96	−26 18 49.5
0034 − 01	3C15	00 34 30.42	−01 25 34.7
0035 − 02	3C17	00 35 47.17	−02 24 09.1
0038 + 09	3C18	00 38 14.76	+09 46 59.5
0045 − 25	NGC253	00 45 05.74	−25 33 39.6
0055 − 01	3C29	00 55 01.57	−01 39 39.7
0114 − 21	OC-224	01 14 25.95	−21 07 54.9
0123 − 01	3C40	01 23 27.49	−01 36 17.2
0131 − 36	NGC612	01 31 43.50	−36 44 56.7
0157 − 31	OC-397	01 57 58.30	−31 07 56.5
0159 − 11	3C57	01 59 30.34	−11 46 59.0
0213 − 13	3C62	02 13 12.20	−13 13 24.6
0305 + 03	3C78	03 05 49.09	+03 55 13.2
0325 + 02	3C88	03 25 18.19	+02 23 20.3
0403 − 13	OF-105	04 03 13.95	−13 16 18.4
0404 + 03	3C105	04 04 38.99	+03 34 27.5
0405 − 12	OF-109	04 05 27.46	−12 19 31.9
0427 − 53		04 27 58.85	−53 56 09.5
0500 + 01	OG3	05 00 45.18	+01 58 53.8
0605 − 08	OH-10	06 05 36.05	−08 34 19.2
0620 − 52		06 20 36.85	−52 40 00.9
0736 + 01	OI61	07 36 42.53	+01 43 59.9
0806 − 10	3C195	08 06 30.29	−10 18 50.2
0825 − 20	OJ-242	08 25 03.54	−20 16 27.7
0834 − 19	OJ-158.1	08 34 56.07	−19 41 25.4
0858 − 27	OJ-297	08 58 31.51	−27 56 33.1
1015 − 31	OL-327	10 15 53.38	−31 29 11.3
1151 − 34	OM-386	11 51 49.44	−34 48 47.1
1216 + 02	3C270	12 16 49.90	+06 06 08.8
1245 − 19	ON176.2	12 45 45.23	−19 42 57.5
1251 − 12	3C278	12 51 58.56	−12 17 52.2
1253 − 05	3C279	12 53 35.84	−05 31 08.1
1306 − 09	OP-10	13 06 02.09	−09 34 33.3
1308 − 22	3C283	13 08 57.35	−22 00 46.2
1318 − 43	NGC5090	13 18 17.40	−43 26 33.4
1333 − 33	IC4296	13 33 47.16	−33 42 39.8
1510 − 08	OR-107	15 10 08.90	−08 54 47.6
1514 + 07	3C317	15 14 16.99	+07 12 17.1
1514 − 24	Ap Lib	15 14 45.27	−24 11 22.6
1518 + 04	4C04.5	15 18 44.70	+04 41 05.5
1559 + 02	3C327	15 59 55.64	+02 06 12.7
1622 − 25	OS-237.8	16 22 44.09	−25 20 51.6
1637 − 77		16 37 05.10	−77 10 08.7
1717 − 00	3C353	17 17 53.28	−00 55 48.7
1733 − 56		17 33 21.43	−56 32 16.3
1839 − 48		18 39 26.20	−48 39 23.1
2008 − 06	OW-15	20 08 33.70	−06 53 01.6
2058 − 28	OW-297.8	20 58 38.68	−28 13 43.9
2104 − 25	OX-208	21 04 29.87	−25 37 50.2
2128 + 04	OX46	21 28 02.61	+04 49 04.5
2128 − 12	OX-148	21 28 52.67	−12 20 20.6
2135 − 14	OX-158	21 35 01.15	−14 46 27.4
2135 − 20	OX-258	21 35 01.33	−20 56 03.7
2203 − 18	OY-106	22 03 25.73	−18 50 17.1
2243 − 12	OY-172.6	22 43 39.79	−12 22 40.3
2314 + 03	3C459	23 14 02.34	+03 48 55.0
2345 − 16	OZ-176	23 45 27.68	−16 47 52.6

843-MHz MOST data are in Jones & McAdam (1992), and 1415-MHz data are in Christiansen et al. (1977).

5 DISCUSSION

A complete discussion of the characteristics of the sample, using both radio and spectroscopic data, will be presented in a forthcoming paper. Here we concentrate on a brief overview of the radio characteristics of the sample.

In column 9 of Table 3 we give a morphological classification of the objects according to their Fanaroff & Riley type. We also indicate the objects that are unresolved (U). To be included in this group, an object must be not only unresolved at the resolution of our data or in the data of comparable resolution collected from literature, but must also have a detected flux density similar to the 'total power' flux density (PW85). This criterion will ensure that the objects classified as U are compact, i.e. at least subgalactic $\theta \leq 30$ kpc. For many objects we could not make a clear classification; these cases are indicated with a question mark in Table 3.

There is some difficulty in the morphological classification because of incomplete or ill-matched *uv* coverage leading sometimes to poorly represented extended source structure. In these cases more data are required to investigate the structure more thoroughly. However, this is not the only problem. Looking at our images, it is clear that the classification suggested by Fanaroff & Riley, even if very effective as a first-order scheme, becomes inadequate given the extremely detailed radio structure that is accessible with modern radio synthesis telescopes. Objects that may be classified as transition cases (like PKS 1333 − 33 where structural details typical of both FR I and FR II can be seen) are also prevalent.

Keeping in mind all the possible uncertainties mentioned above, we can summarize the morphological classification as 41 FR II, 19 FR I and 31 U, while the rest are uncertain cases or objects with too complex a structure. If we restrict this analysis to the 'complete sample' (the 87 objects with $z<0.7$), we find 36 FR II (41 per cent), 19 FR I (22 per cent) and 15 U (17 per cent).

With the necessary precautions, these results can be compared with those obtained by Peacock & Wall (1981 [PW81], 1982) for a similar sample of radio sources in the Northern Hemisphere. Restricting that sample to the sources with $z<0.7$ (but note that many objects in PW81 do not have a redshift measurement), the percentage of FR I (~ 13 per cent) is lower than in our sample while the fraction of FR II (~ 50 per cent) is higher. The percentage of unresolved sources is also larger in PW81 at ~ 28 per cent, while the number of unclassified sources is lower. Part of these discrepancies may be due to the better sensitivity of our maps that allowed the detection of more structural details, but it is interesting to have a closer look at the group of unresolved sources and in particular at the so-called compact steep-spectrum (CSS) radio sources. As already noticed by Peacock & Wall (1982), such sources are very common in samples selected at high frequencies compared to samples selected at low frequencies (e.g. 3CR) where the majority of compact sources have a flat spectrum. These CSS objects have subgalactic apparent radio dimensions and $\alpha > 0.5$ (with $S = \nu^{-\alpha}$), and they are believed to be intrinsically small sources rather than extended sources shortened by projection effects (Fanti et al. 1990).

In our complete sample we find that, among the unresolved objects, seven are CSS sources (8 per cent of the sample). This number has to be compared with the 13 per cent of CSS sources observed in the PW81 sample restricted to $z<0.7$. On the other hand, if we consider our whole observed sample (which is not statistically complete but includes also objects with $z>0.7$), we find that the percentage of CSS sources already increases to 18 per cent (20 CSS sources observed) and in a similar way the percentage of CSS sources increases to 22 per cent if we analyse the whole PW81 sample. Both samples then show a similar trend (an increase in the percentage of CSS sources) when sources at high redshift are included in the statistic. This supports the idea (Kapahi & Kulkarni 1990; Onuora 1992) that the number of these objects seems to depend strongly on redshift. This redshift-dependence may also be the reason that the CSS sources form the majority of the objects for which we could not find an optical identification (see Paper III).

In Fig. 4 we plot the distribution of the total power for the two morphological groups, FR I and II. This was done using only the objects included in the 'complete sample'. As is well known, the FR I group shows, on average, a lower radio power (median value log $P_{\rm tot}$(4.8 GHz)$=25.13$) than the FR II (median value log $P_{\rm tot}$(4.8 GHz)$=26.28$). It is clear from the plot, however, that the transition between the two groups is smooth, and a large region of overlap exists.

Fig. 5 shows the distribution of the orientation parameter, R, again for FR I and FR II classes. The median value is log $R=-1.77$ for FR II and log $R=-1.44$ for FR I. Applying Gehan's generalized Wilcoxon test, and taking the upper limits into account (using ASURV Rev 1.1, LaValley, Isobe & Feigelson 1992), we find a probability of about 8 per cent for the distributions to be different. Considering the uncertainties in the classification (note that the two FR I with a lower value of R are Fornax A and Hercules A), there is a mild indication that FR I have larger values of R than FR II. This difference possibly reflects the fact that, for radio galaxies, the radio core power does not increase linearly with the total power (Feretti et al. 1984).

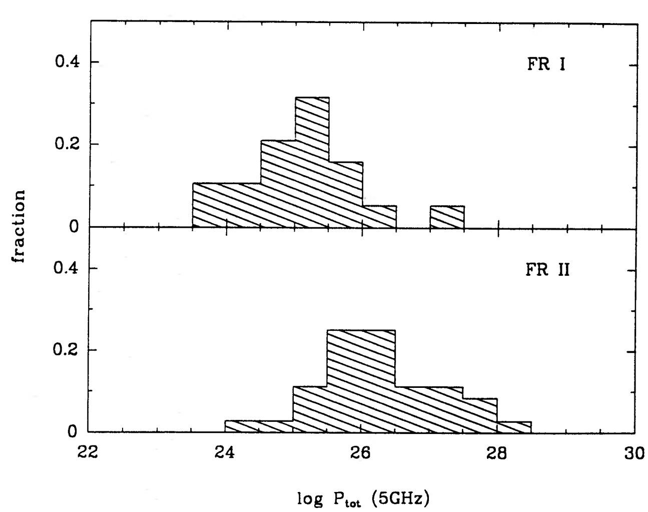

Figure 4. Histogram of the total power (WP85) for the FR I and FR II groups.

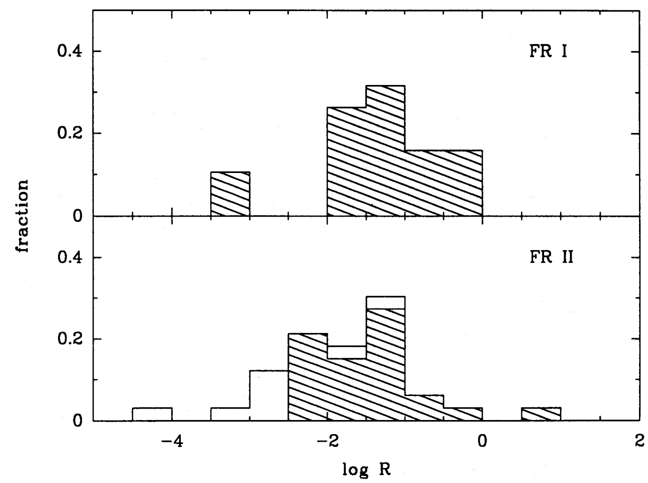

Figure 5. Histogram of the orientation parameter, R, for the FR I and FR II classes. The dashed areas are the histograms for the detections, while the open areas indicate upper limits.

ACKNOWLEDGMENTS

We are grateful to Ann Burgess, Marco Costa, Eric Feigelson, Dick Hunstead, Anton Koekemoer and Rick Perley, who contributed data or information prior to publication.

REFERENCES

Baars J. W. M., Genzel R., Pauliny-Toth I. I. K., Witzel A., 1977, A&A, 61, 99
Baum S. A., Heckman T., 1989, ApJ, 336, 702
Baum S. A., Heckman T., Bridle A. H., van Breugel W., Miley G., 1988, ApJS, 68, 643
Bridle A. H., Perley R. A., 1984, ARA&A, 22, 319
Browne I. W. A., Clark R. R., Moore P. K., Muxlow T. W. B., Wilkinson P. N., Cohen M. H., Porcas R. W., 1982, Nat, 299, 788
Burns J. O., Feigelson E. D., Schreier E. J., 1983, ApJ, 273, 128
Christiansen W. N., Frater R. H., Watkinson A., O'Sullivan J. D., Lockhart I. A., Goss W. M., 1977, MNRAS, 181, 183
Clark B. G., 1980, A&A, 89, 377
Conway J. E., Cornwell T. J., Wilkinson P. N., 1990, MNRAS, 246, 490
Conway R. G., Stannard D., 1972, MNRAS, 160, 31P
Danziger I. J., Fosbury R. A. E., Goss W. M., Ekers R. D., 1979, MNRAS, 188, 415
Danziger I. J., Fosbury R. A. E., Goss W. M., Bland J., Boksenberg A., 1984, MNRAS, 208, 589
Dreher J. W., Feigelson E. D., 1984, Nat, 308, 43
Duncan R. A., 1992, ATCA Calibrator List. ATNF Internal Doc., Australia Telescope National Facility, CSIRO
Duncan R. A., Sproats L. N., 1992, Proc. Astron. Soc. Aust., in press
Ekers R. D., Goss W. M., Kotanyi C. G., Skellern D. J., 1978, A&A, 69, L21
Ekers R. D., Goss W. M., Wellington K. J., Bosma A., Smith R. M., Schweizer F., 1983, A&A, 127, 361
Ekers R. D. et al., 1989, MNRAS, 236, 737
Fanaroff B. L., Riley, J. M., 1974, MNRAS, 167, 31P
Fanti R., Fanti C., Schilizzi R. T., Spencer R. E., Nan Rendong, Parma P., van Breugel W. J. M., Venturi T., 1990, A&A, 231, 333

Feretti L., Giovannini G., Gregorini L., Parma P., Zamorani G., 1984, A&A, 139, 55
Fomalont E. B., Ebneter K. A., van Breugel W. J. M., Ekers R. D., 1989, ApJ, 346, L17
Fosbury R. A. E., Bird M. C., Nicholson W., Wall J. V., 1987, MNRAS, 225, 761
Fosbury R. A. E., di Serego Alighieri S., Corvoisier T. J.-L., Snijders M. A. J., Walsh J., Wilson W. E., 1990, IUE Astronomy in the Era of New Space Missions. ESA SP-310, European Space Agency
Goss W. M., Danziger I. J., Fosbury R. A. E., Boksenberg A., 1980, MNRAS, 190, 23P
Jackson N., Browne I. W. A., 1991, MNRAS, 250, 422
Jones P. A., McAdam W. B., 1992, ApJS, 80, 137
Junkes N., Haynes R. F., Harnett J. I., 1992, in Duschl W. J., Wagner S. J., eds, Physics of Active Galactic Nuclei. Springer-Verlag, Berlin, p. 570
Kapahi V. K., Kulkarni V. K., 1990, AJ, 99, 1397
Keel W. C., 1986, ApJ, 302, 296
Killeen N. E. B., Bicknell G. V., 1988, ApJ, 324, 198
Killeen N. E. B., Bicknell G. V., Ekers R. D., 1986, ApJ, 302, 306
Kronberg P. P., Wielebinski R., Graham D. A., 1986, A&A, 169, 63
La Valley M. P., Isobe T., Feigelson E. D., 1992, BAAS, 24, 839
Mantovani F., Junor W., Fanti R., Padrielli L., Browne I. W. A., Muxlow T. W. B., 1992, MNRAS, 257, 353
Morganti R., Ulrich M.-H., Tadhunter C. N., 1992, MNRAS, 254, 546
O'Dea C. P., Owen F. N., 1985, AJ, 90, 927
O'Dea C. P., Baum S. A., Stanghellini C., 1991, ApJ, 380, 66
Onuora L. I., 1992, ApJ, 386, 452
Owen F. N., O'Dea C. P., Inoue M., Eilek J. A., 1985, ApJ, 294, L85
Peacock J. A., Wall J. V., 1981, MNRAS, 194, 331
Peacock J. A., Wall J. V., 1982, MNRAS, 198, 843
Prestage R. M., 1985, PhD thesis, Univ. Edinburgh
Prieto M. A., Walsh J. R., Fosbury R. A. E., di Serego Alighieri S., 1993, MNRAS, 263, 10
Rawlings S., Saunders R., Eales S. A., Mackay C. D., 1989, MNRAS, 240, 701
Saikia D. J., Subrahmanya C. R., Patnaik A. R., Unger S. W., Cornwell T. J., Graham D. A., Prabhu T. P., 1986, MNRAS, 219, 545
Sault R. J., 1991, Some Simulations of Self-calibration for the AT. ATNF Technical Memorandum, Australia Telescope National Facility, CSIRO
Sault R. J., 1992, Multi-frequency Synthesis with the ATCA. ATNF Technical Memorandum, Australia Telescope National Facility, CSIRO
Sault R. J., Killeen N. E. B., Kesteven M. J., 1991, AT Polarization Calibration. ATNF Technical Memorandum, Australia Telescope National Facility, CSIRO
Schwab F. R., 1980, SPIE Proc., 231, 18
Tadhunter C. N., Morganti R., di Serego Alighieri S., Fosbury R. A. E., Danziger I. J., 1993, MNRAS, 263, 999 (Paper I, this issue)
Taylor G. B., Perley R. A., Inoue M., Kato K., Tabara H., Aizu K., 1990, ApJ, 360, 41
Ulrich M.-H., 1978, ApJ, 219, 424
Ulvestad J. A., Neff S. G., Wilson A. S., 1987, AJ, 93, 22
Unger S. W., Booler R. V., Pedlar A., 1984, MNRAS, 207, 679
Walker R. C., Benson J. M., Unwin S. C., 1987, ApJ, 316, 546
Wall J. V., Peacock J. A., 1985, MNRAS, 216, 173 (WP)